Q7
3-29-83

(1)

I-8531

SAND--83-0082

DE83 009387

HIGH-ENERGY GAS-FRACTURING DEVELOPMENT

QUARTERLY REPORT
(October 1 - December 31, 1982)

Prepared by
J. F. Cuderman
Sandia National Laboratories
Box 5800
Albuquerque, New Mexico 87185

SAND83-0082

for

GAS RESEARCH INSTITUTE
Contract No. 5080-321-0434

GRI Project Manager
Timothy D. Kurtz
Devonian Shale Research

February 1983

Gas Research Institute
8600 West Bryn Mawr Avenue
Chicago, Illinois 60631

DISCLAIMER

HIGH-ENERGY GAS-FRACTURING DEVELOPMENT

QUARTERLY REPORT
(October - December 1982)

Prepared by

J. F. Cuderman
Sandia National Laboratories
Box 5800
Albuquerque, NM 87185

SAND83-0082

For
GAS RESEARCH INSTITUTE
Contract No. 5080-321-0434

GRI Project Manager
Timothy D. Kurtz
Devonian Shale Research

February 1983

GRI DISCLAIMER

RESEARCH SUMMARY

Title	High Energy Gas Fracturing Development
Contractor	Sandia National Laboratories GRI Contract Number: 5080-321-0434
Principal Investigator	J. F. Cuderman
Report Period	October-December 1982 Quarterly Report
Objective	To develop and optimize the High Energy Gas Fracturing (HEGF) technique to produce multiple fractures around a wellbore in order to stimulate natural-gas production in Devonian shale.
Technical Perspective	Most gas wells in Devonian shales require stimulation to obtain commercially economic production. Traditionally this has been done with high explosives, and more recently with hydraulic and foam fracturing. However, high explosives can produce a crushed, compacted region in the immediate vicinity of the wellbore that can effectively seal off production. The HEGF technique uses a wellbore charge of a propellant tailored to produce pressure loading in the borehole that avoids crushing yet produces multiple fractures radiating from the wellbore. Work to date has developed an understanding of multiple fracturing by propellant deflagration. The multiple-fracture regime has been characterized and related to parameters such as borehole size, pressure risetime, and surface-wave velocity. Pressure risetimes and peak pressures, measured for different propellants in boreholes of varying diameters, have made it possible to specify a propellant for a desired peak pressure and pressure risetime. Semiempirical models, using results from previous experiments, successfully relate stress, acceleration, and fracture radii in surrounding rock to peak pressure and pressure risetime. A finite-element model also has been developed which predicts fracture type and direction of fractures as a function of pressure loading, in situ stress, and material properties. A full-scale HEGF system has been developed for application in gas-well-stimulation experiments in Devonian shale.
Results	During this quarter, a proof test of the full-scale HEGF system was conducted at the Nevada Test Site (NTS). The designed pressure pulse of 0.5 ms risetime was achieved, and the tamp remained in place during the test. The borehole was successfully cleared

posttest. Multiple fracturing was verified with a downhole TV camera. The test of the full-scale hardware and its operational capability was successful. As a result, the HEGF system is ready for application in gas-well-stimulation experiments in Devonian shale.

An important aspect of the HEGF-development program was to establish safe handling procedures for propellant, ignitors, and propellant-canister segments. Tests were conducted to determine worst-case accident scenarios to establish sensitivity to shock and fire. There appears to be no risk of initiation resulting from shock or breakage of the propellant-canister segments. The burning of propellant-canister segments does not appear to result in consequences significantly more severe than the flash fire resulting from an equal amount of unconfined propellant being burned.

Technical Approach

The HEGF program has consisted of three parts: (1) in situ experiments at NTS, (2) modeling activities, and (3) full-scale experiments in Devonian shale. The in situ experiments served to determine peak pressures and pressure risetimes as a function of propellant type and borehole diameter. They also served to verify model predictions, to develop a workable tamp design, and to test prototype hardware being developed for experiments in Devonian shale. The in situ experiments were conducted both in a tunnel complex and in existing vertical boreholes. The tunnel experiments permitted mineback for direct observation of fracturing obtained. Modeling activities consisted of both semiempirical modeling, used to predict fracture regimes for instrument settings, and finite-element modeling, used to analyze experimental results and predict fracture geometry. Both the modeling effort and the in situ experiments were directed toward the design of experiments in Devonian shale planned for the spring of 1983. The hardware and operational capability for those experiments were proof-tested in a vertical borehole at NTS during this quarter.

TABLE OF CONTENTS

TABLES

ILLUSTRATIONS

1. OVERALL OBJECTIVE OF THE PROGRAM

The overall objective of the High Energy Gas Fracture (HEGF) development program is to develop and optimize the HEGF technique to produce multiple fractures about a wellbore in order to stimulate natural-gas production in Devonian shale.

2. CURRENT YEAR (APRIL 1982 - MARCH 1983)

2.1 Specific Objectives for Current Year

2.1.1 In Situ Experiments

Develop hardware and tamp technique for full-scale HEGF experiments in Devonian shale.

2.1.2 Finite-Element Modeling

Continue development of finite-element models to improve analysis of fracture behavior.

2.1.3 Full-Scale Experiments

Perform full-scale experiments using the HEGF technique in Devonian-shale gas wells.

2.2 Work Plan (Tasks) for Current Year

2.2.1 In Situ Experiments

Develop a tamp design and emplacement method that contains the propellant burn and leaves the instrument and messenger cables and residual hardware in place for facilitating posttest removal.

Conduct a test of tailored-pulse loading in Eleana argellite (a second lithology more closely resembling Devonian shale).

2.2.2 Finite-Element Modeling

Refine the treatment of plastic flow and incorporate propellant-burn and gas-dynamic models into the finite-element analysis.

2.2.3 Full-Scale Experiment

2.2.3.1 Hardware Design and Fabrication -- Design and fabricate hardware to be used in the full-scale experiment in Devonian shale.

2.2.3.2 Component Testing -- Test individual components and improve designs where necessary.

2.2.3.3 Proof Test of Hardware at NTS

2.2.3.4 Full-Scale Experiments in Devonian Shale

2.2.3.5 Safety Evaluation -- Perform drop tests and burn tests of the propellant canister to establish safe handling procedures for the propellant, rapid ignition propagation (RIP) ignitors, and assembled propellant-canister segments.

2.2.3.6 Gap Tests -- Conduct tests to determine the maximum acceptable separation, or gap, between individual propellant-canister segments so that the RIP ignitor in one segment successfully initiates the RIP ignitor in the one below it.

3. PREVIOUS QUARTER (JULY - SEPTEMBER 1982)

3.1 Work Performed during Previous Quarter

3.1.1 Tamp Development

A stemming scheme was devised whereby a roughly 12-foot (3.7-m) section of dry Overton (Nevada) sand was capped by a 2-foot (0.6-m) plug of fast-setting, sulfate-based cement ($2CaSO_4 \cdot H_2O$) and sand (50/50 mixture). A squib-activated tamp-emplacement canister was designed to deliver sand, cement/sand mixture, and water to the desired depth in the borehole.

3.1.2 Incorporation of Plastic Flow in the Finite-Element Model

Previous finite-element calculations of gas fracture used a material model with a tensile-fracture criterion and elastic behavior in compression.[1] Since it is likely that material would flow plastically under high loading rates, the inclusion of plasticity provides a better qualitative correspondence to observed experimental results at high loading rates. As a result, scoping calculations with both plasticity and tensile fracture were incorporated into the finite-element model.

3.2 Conclusions from Previous Quarter's Work

3.2.1 Tamp Development

Tamp development tests indicate that (1) dry sand cannot be reliably emplaced from the surface in a damp wellbore of even a few hundred feet depth, (2) the cement/sand plug must be used to retain the package in place, and (3) the exterior of the cable tube must be roughened to improve adhesion between the sand tamp and the cable tube. Because the water was allowed to permeate into the cement/sand plug overnight after emplacement, there was minimal upward motion of the experiment package during the propellant burning.

3.2.2 Incorporation of Plastic Flow in the Finite-Element Model

Modeling plastic flow in materials subjected to high dynamic-loading rates improves accuracy in predicting fractures resulting from borehole pressurization. The new calculations provide a better qualitative correspondence to the observed experimental results at high loading rates.

4. CURRENT QUARTER (OCTOBER - DECEMBER 1982)

4.1 Work Planned for Current Quarter

4.1.1 Proof Test of System for Full-Scale Experiment

Proof-test the entire hardware package that will be used in the full-scale experiments in Devonian shale. The proof test is to be conducted in a 6-3/4-in (0.17-m) diameter borehole in ash-fall tuff at the Nevada Test Site (NTS).

4.1.2 Safety Evaluation

Perform drop tests and burn tests of the propellant canister to establish safe handling procedures for the propellant, RIP ignitors, and assembled propellant-canister segments.

4.1.3 Refinements to the Semiempirical Model and Its Applications

Refine semiempirical equations that predict the conditions required for multiple fracturing to include the influence on pressure risetime of increased free volume (canister void space plus annular volume between canister and borehole). The refined model is applied in specifying a propellant mixture that produces multiple fracturing in the proof test.

4.2 Work Actually Performed during Current Quarter

4.2.1 Proof Test of System for Full-Scale Experiment

A proof test of the full-scale package was conducted at NTS on October 27, 1982. A 6-3/4-inch (0.17-m) diameter borehole in ash-fall tuff (total depth = 361 ft [110 m]) was backfilled with pea gravel to a depth of 238 ft (72.5 m). The test package included a 96.20-ft (29.32-m) long propellant canister, a 3.50-ft (1.06-m) long firing module/pressure-transducer canister, a 19.34-ft (5.89-m) long cable tube, and a 26.88-ft (8.19-m) long tamp-emplacement canister (Figure 1). The entire package weighed approximately 1550 lb (700 kg).

The propellant canister consisted of 12 segments, each 8 ft (2.4 m) long. It contained 769 lb (349 kg) of M5 propellant, in a mixture by weight of 20% smaller-grained M5(A) and 80% larger-grained M5(B). The composition of the mixture was determined on the basis of results from previous experiments but was adjusted for the 2.5-times-greater free volume of the proof-test borehole compared with the borehole used in the GF4 experiment (see Section 4.2.3). Figure 2 is a schematic of a single propellant-canister segment. Each segment consisted of a section of 5-5/8-in (0.14-m) OD polyvinyl chloride (PVC) tubing, two threaded PVC mating endcaps, and a centered RIP ignitor. The RIP ignitor consisted of 1/2-in (0.013-m) diameter PVC tubing that contained a mild-detonating fuse (MDF) surrounded by $BKNO_3$ along its length. The ends of the MDF terminated with a 1/8-in diameter flyer-plate assembly in close proximity to a similar plate in the next canister in the train. Thus each RIP ignitor initiates the one below it. The propellant filled the annulus between the RIP ignitor and the 5-5/8-in (0.14-m) OD PVC tubing. The canister design is such that the endcaps shield the ends of the RIP ignitor. This allows the canisters to be placed on end for easier loading, protects them from damage, and enhances safety. PVC was selected for the canister material because it shatters on sudden pressurization, is readily available, and is economical. Moreover, standard 5-in PVC tubing has sufficient strength to support several hundred feet of joined propellant-canister

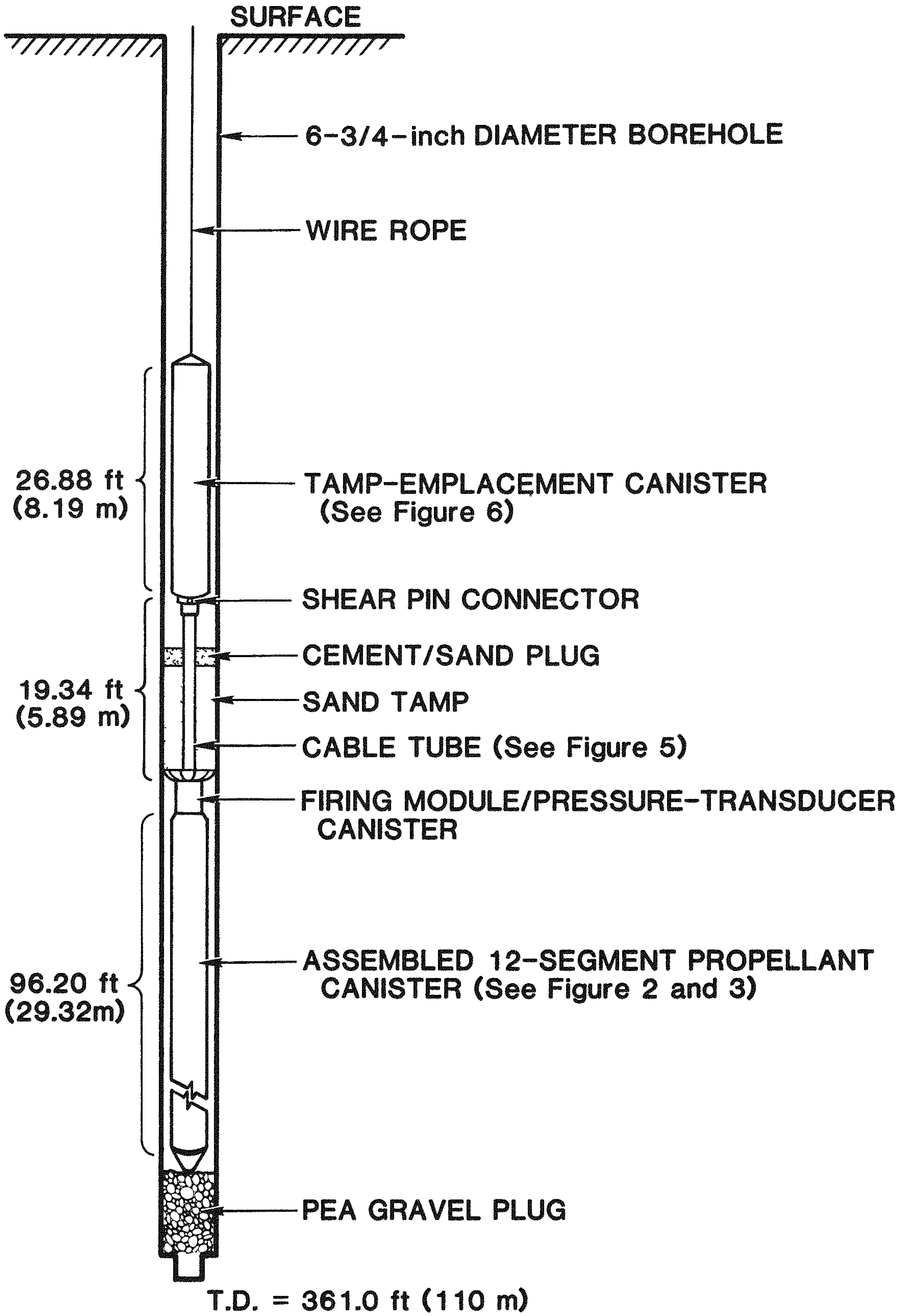

Figure 1. Schematic of Proof-Test Downhole Hardware

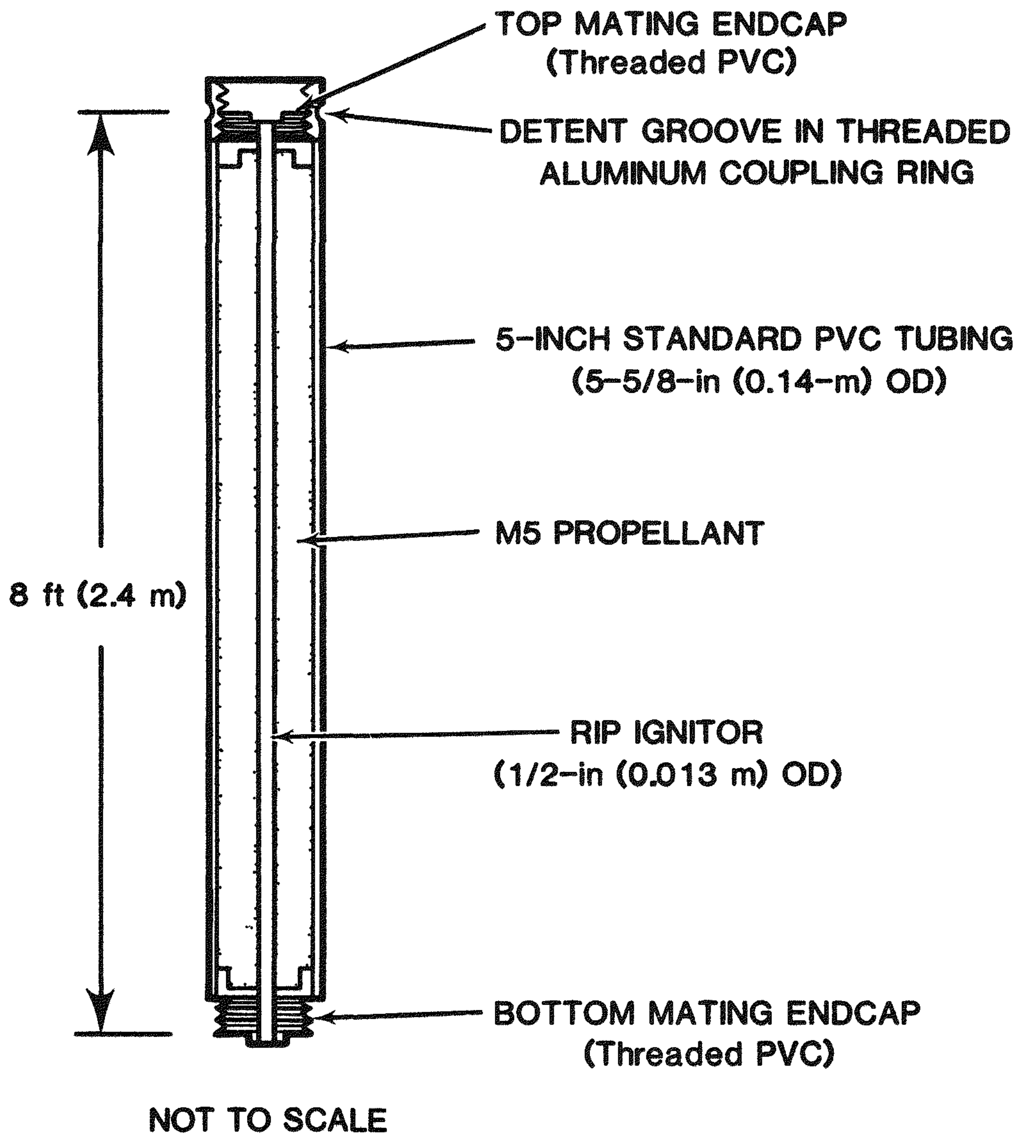

Figure 2. Schematic of Propellant Canister Segment

segments. The bottom of the first segment was capped with a nose cone. Individual propellant-canister segments were mated by threaded aluminum coupling rings. A detent groove in the coupling ring enabled each topmost propellant-canister segment of the downhole train to be clamped and supported while the next segment was being attached. A small assembly containing two exploding-bridge-wire (EBW) initiators, in contact with a strip of MDF, was attached to the top of the final propellant-canister segment, so that the MDF mounted flush against the top end of the last RIP ignitor. The EBW initiators, and in turn the MDF and the topmost RIP ignitor, were ignited by high-voltage output from the firing module (Figure 3). Figure 4 is a sequence of photographs showing the propellant-canister hardware and installation.

The firing module/pressure-transducer canister, made of aluminum, mounted directly above the EBW initiators and directly below the stemming-feedthrough cable tube (Figure 5). The cable tube was 2-in (0.051-m) OD, 0.25-in (0.0064-m) wall, aluminum tubing, the surface roughened by sandblasting to improve adhesion between the sand tamp and the cable tube. This, together with circular ribs welded to the exterior of the tube, prevented the cable tube from moving vertically during the test. An electrical messenger cable from the firing module/pressure-transducer canister was run up through the tube and terminated in a connector at its top. The cable-tube connector mated with a detachable connector at the lower end of the primary cable--a nine-pair cable that ran through the tamp-emplacement canister. The tamp-emplacement canister and cable-tube supports were joined by a shear-pin connector designed to shear with a 6000-lb (2700-kg) pull. The top of the tamp-emplacement canister (Figure 6) was fastened to a wire rope from which the entire assembly was suspended and lowered from the surface. Figure 7 shows the installation of the cable tube and tamp-emplacement canister.

After being suspended in the hole, the lower compartment of the tamp-emplacement canister was filled with sand and topped with a 50/50 mixture of fast-setting, sulfate-based cement ($2CaSO_4 \cdot H_2O$) and sand. The upper compartment was filled with 1 gallon (0.004 m^3) of water.

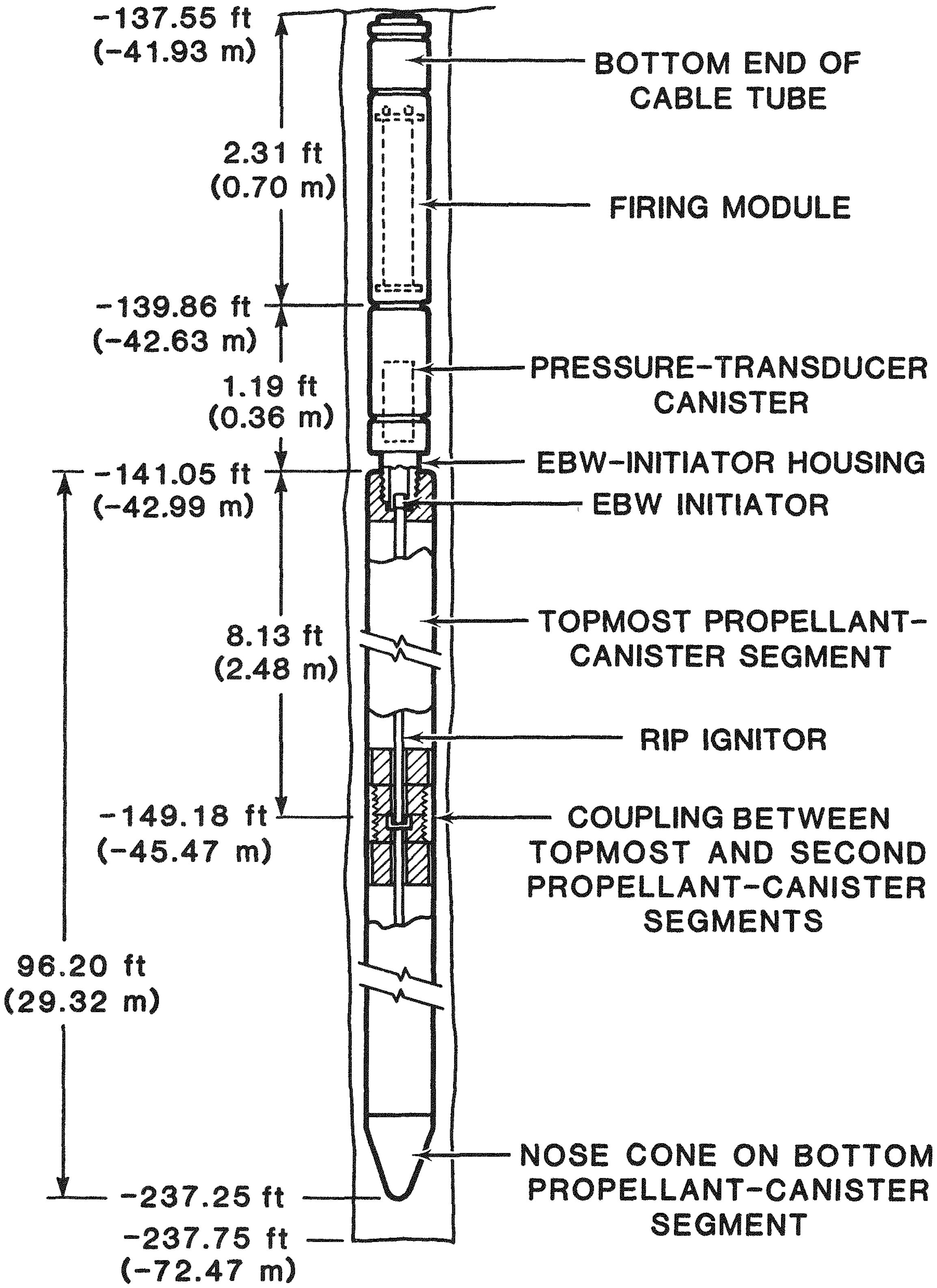

Figure 3. Schematic of Firing Module/Pressure-Transducer Canister and Assembled Propellant Canister

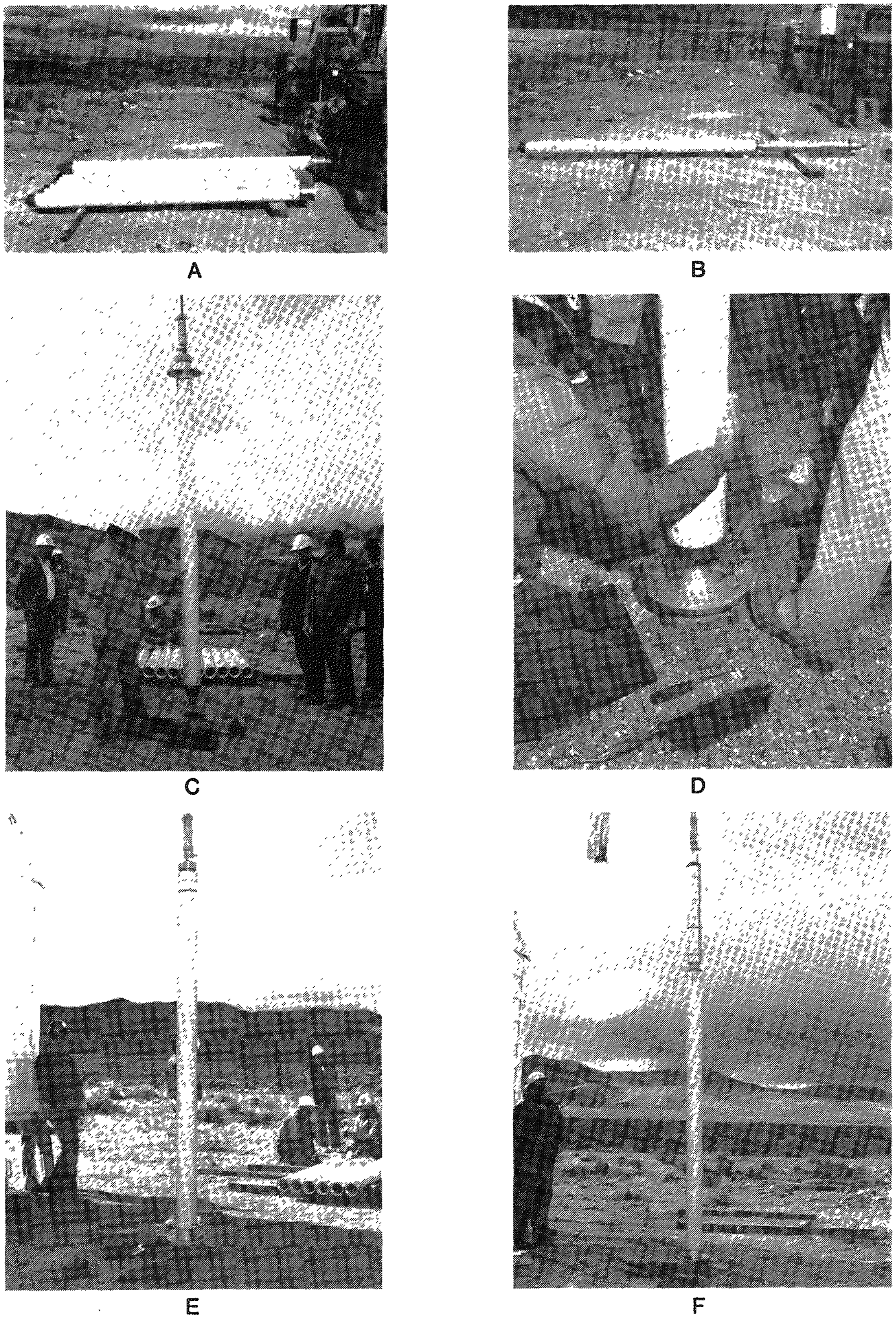

Figure 4. Photographs of Propellant-Canister Installation

(A) Propellant-canister segments ready for installation. The segment with a nose cone is the first to be installed.

(B) Topmost propellant-canister segment connected to firing module/-pressure-transducer canister.

(C) Installation of first propellant-canister segment (note the safety plate that clamps against the detent groove in the aluminum coupling ring).

(D) Intermediate propellant-canister segment screwed together with one previously installed.

(E) Intermediate segment ready to be lowered. Set screws in aluminum coupling ring prevent separation after segments are screwed together and lowered downhole.

(F) Topmost propellant-canister segment, including firing module/-pressure-transducer canister, ready to be lowered.

Figure 4

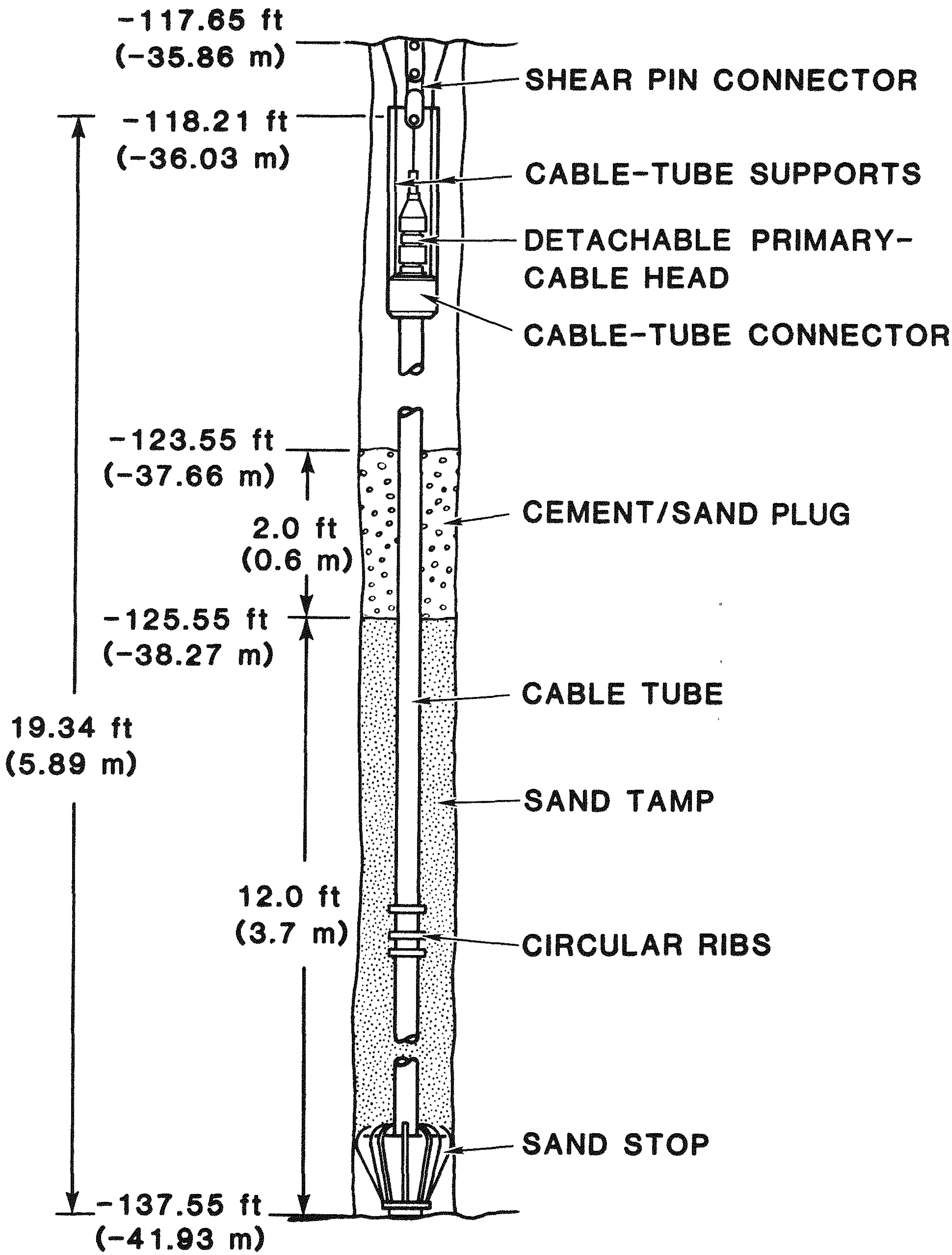

Figure 5. Schematic of Cable Tube with Sand Tamp in Place

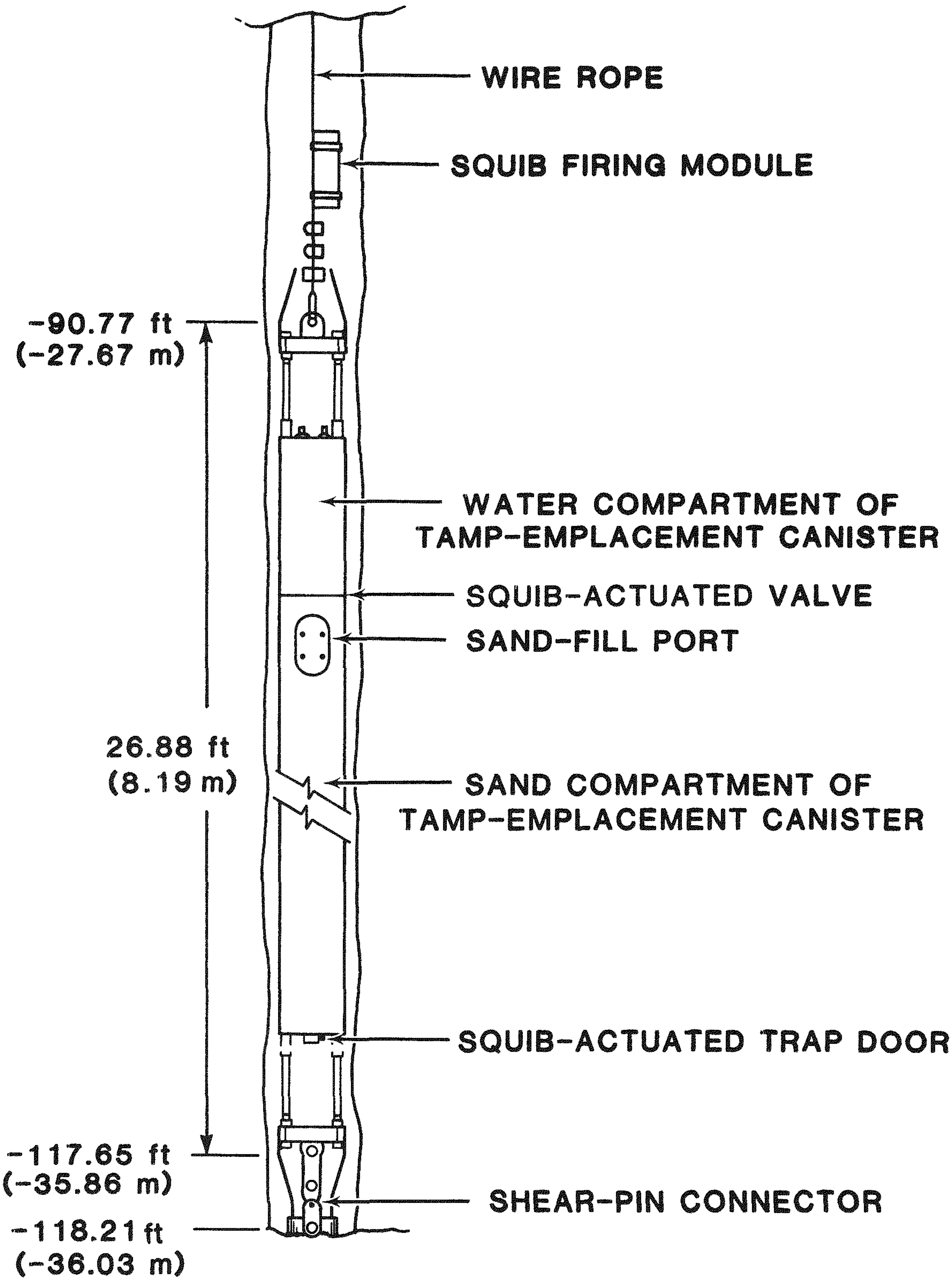

Figure 6. Schematic of Tamp-Emplacement Canister

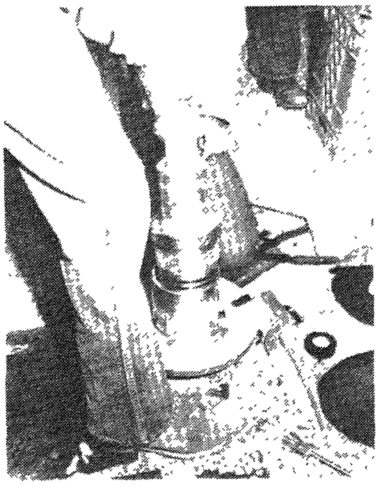

(A) Installation of cable tube (note O-rings to exclude moisture; all connections including those between propellant-canister segments are similarly designed).

(B) Sand stop in place at the lower end of the cable tube (prevents sand from filling the propellant canister/borehole annulus).

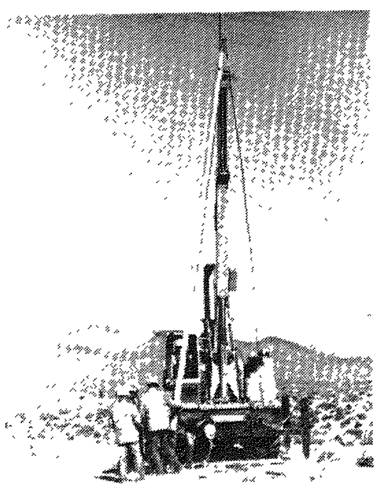

(C) Installation of tamp-emplacement canister. The tamp-emplacement canister is attached to the shear-pin connector after being raised into position.

Figure 7. Photographs of Cable-Tube and Tamp-Emplacement-Canister Installation

The package was lowered and suspended from the top of the casing when the propellant-canister nose cone reached the top of the pea-gravel plug (240-ft [73-m] depth). Electric squibs in the tamp-emplacement canister were fired through a secondary two-pair cable from the surface to release first the sand and cement/sand mixture and then the water. A sand stop at the lower end of the cable tube prevented the sand from filling the propellant-canister/borehole annulus. The resulting tamp was designed to provide 12 ft (3.7 m) of sand tamp capped by 2 ft (0.6 m) of cement/sand mixture. The experiment was left in the borehole overnight to permit water permeation and "set-up" of the cement/sand plug.

The 20/80 mixture by weight of M5(A)/M5(B) propellants was determined to produce multiple fracturing in the ash-fall tuff surrounding the borehole. Ignition of this mixture was calculated to yield a pressure pulse whose risetime would be in the range of 0.4 to 0.7 ms with a peak pressure in the 10,000 to 30,000 psi (70 to 210 MPa) range. Figure 8 is a plot of pressure versus time during the test. The first peak was regarded as the relevant peak for determining fracture behavior. It is believed that the break in the pressure risetime coincided with fracture formation and accompanying free-volume increase. Figure 8 shows that the peak pressure was 16,000 psi (110 MPa), and the pressure risetime was 0.5 ms. An acceleration of about 1.2 g (11.8 m/s^2) was measured on the surface at the borehole. The tamp was successfully retained.

A workover rig and washover tool, as shown in Figure 9, were used for posttest hardware recovery. The tamp-emplacement canister was easily retrieved, because the shear pin had sheared during the experiment (probably because of a standing wave induced by the shot). The cement/sand plug and sand tamp were removed by compressed air, using the washover tool. The cable tube broke off where it mated with the firing module and was retrieved by the washover tool. Figures 10A through 10C show the recovered cable tube. The remainder of the firing module and the pressure transducer were retrieved with the fishing tool shown in Figure 10D. Figures 10E and 10F show recovered

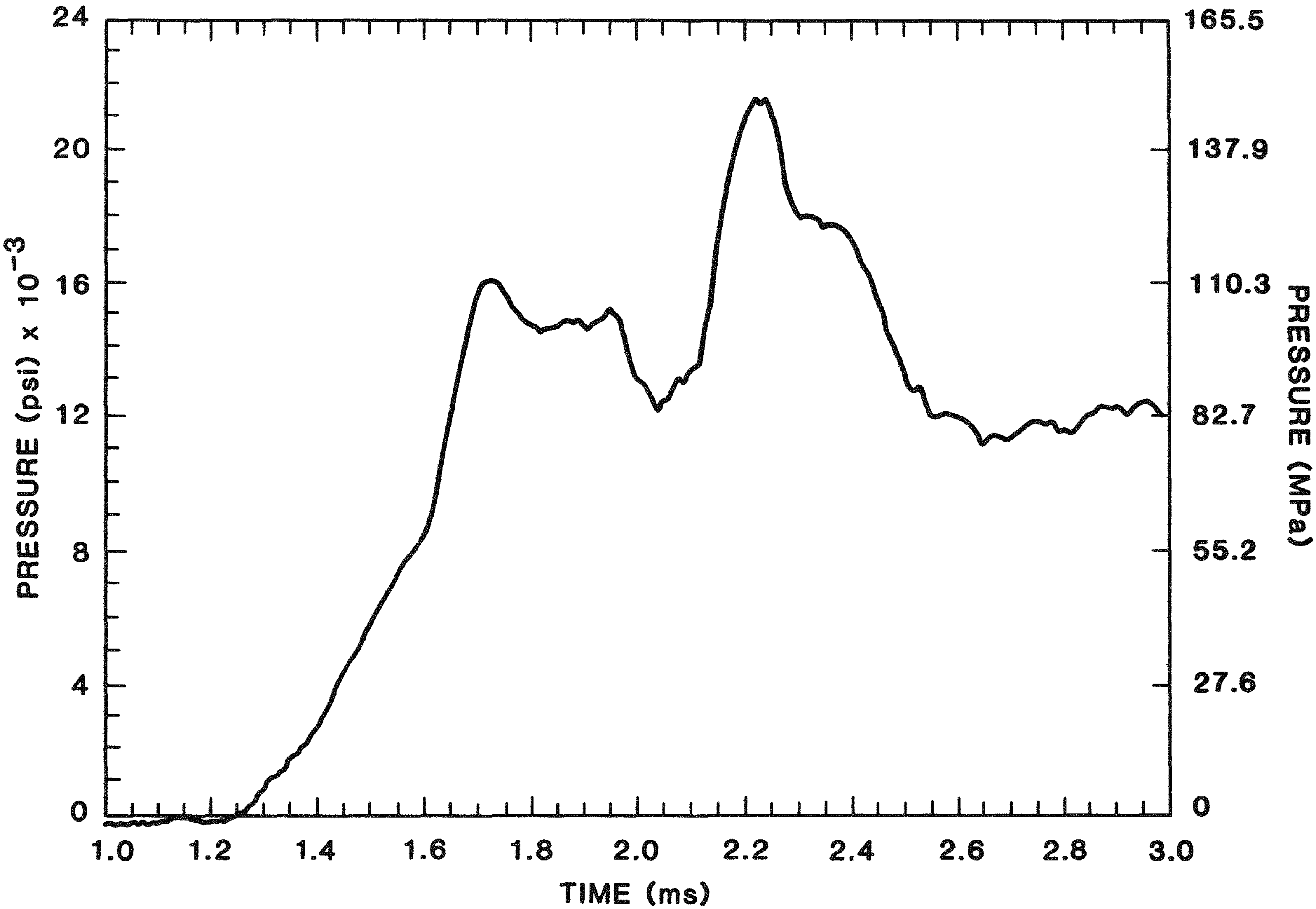

Figure 8. Plot of Pressure vs. Time during Proof Test

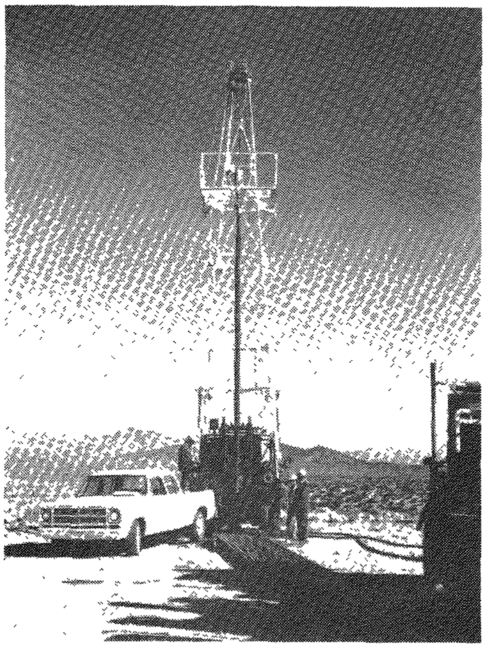

(A) Workover rig with washover tool ready to go downhole.

(B) Washover tool showing wire-rope catchers brazed in the tubing (to snag downhole hardware after removing sand tamp using compressed air).

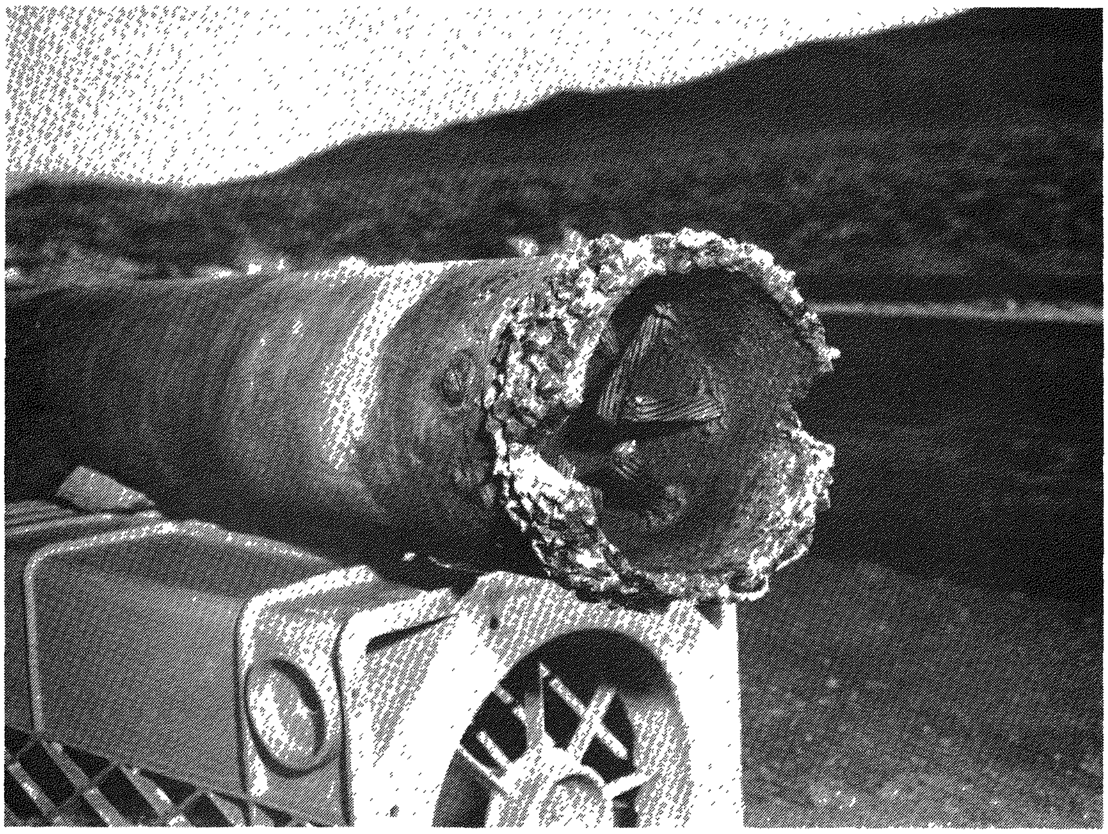

Figure 9. Photographs of Stemming-Removal Equipment

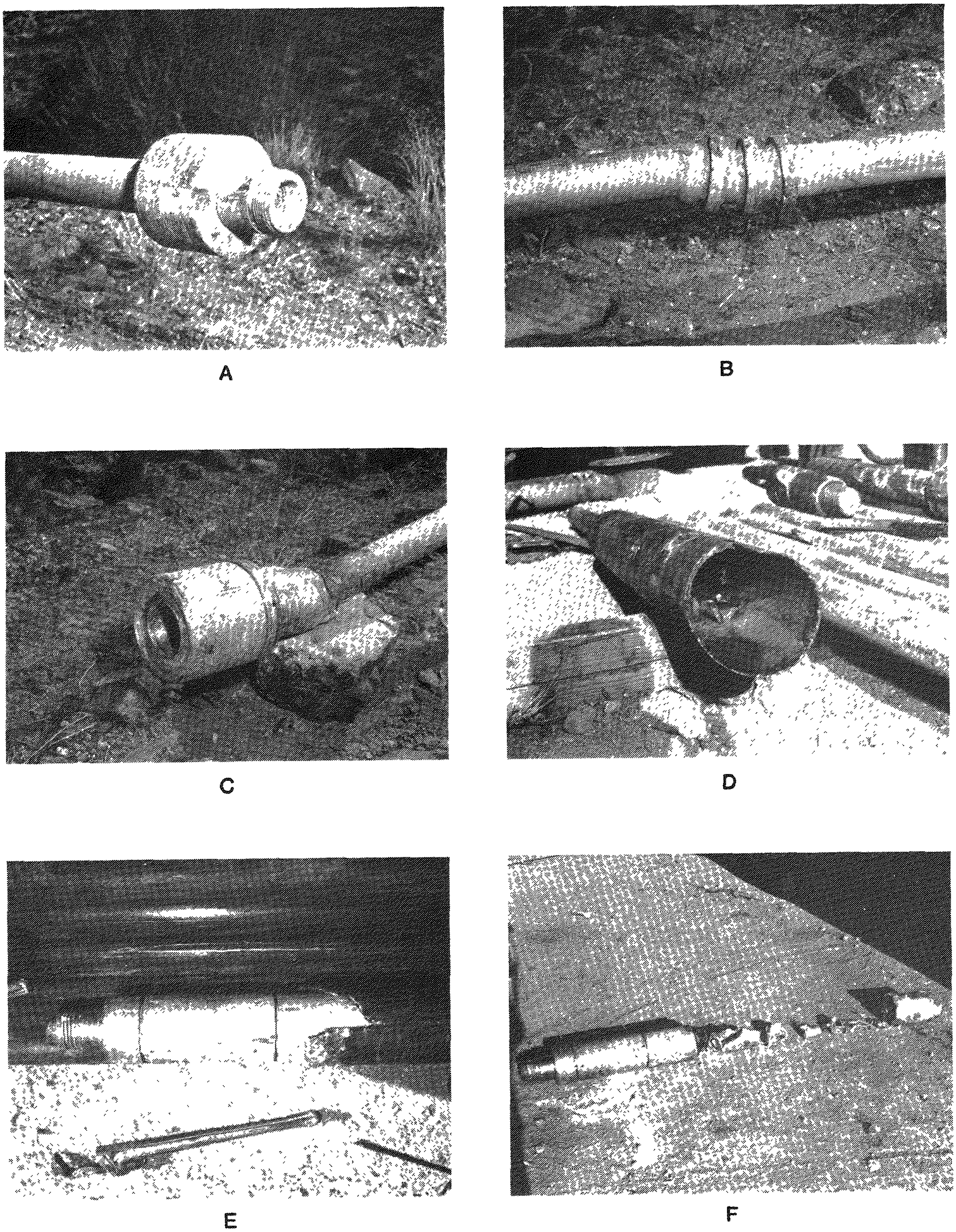

Figure 10. Photographs of Recovered Hardware

(A) Top end of cable tube (minus top supports) showing connector.

(B) Center section of cable tube showing extrusion that probably occurred during the shot; the circular ribs seen here, together with sandblasting of the cable tube, served to maximize adhesion between the sand tamp and the cable tube.

(C) Recovered bottom end of cable tube.

(D) Fishing tool for recovery of firing module/pressure-transducer canister.

(E) Recovered lower half of the firing module/pressure-transducer canister still attached to the fishing tool.

(F) Overview of recovered parts from firing module/pressure-transducer canister.

Figure 10

parts. After recovery of this hardware, a drill bit was installed and the drill stem lowered to a position about 8 ft (2.4 m) below the depth where the pressure transducer was retrieved. At this point an obstruction was encountered. The obstruction was drilled out, and the drill string was taken downhole to a depth of 241 ft (73.5 m) without encountering further major obstructions.

After borehole cleanup, downhole TV scans showed typically 6 to 8 vertical fractures, confirming that multiple fracturing was achieved. Figure 11 is two frames from the downhole TV camera, one showing the wellbore before the test and the other the posttest fractured borehole.

This test of the full-scale hardware and its operational capability was successful. As a result, the system is ready for application in gas-well-stimulation experiments in Devonian shale.

4.2.2 Safety Evaluation

An important aspect of the hardware-development program has been to establish safe handling procedures for the propellant, RIP ignitors, and individual propellant-canister segments. Tests have been conducted to determine the behavior of a propellant-canister segment when dropped or when exposed to fire.

4.2.2.1 Drop Tests -- Drop tests were conducted to test sensitivity to impact. Propellant-canister segments were dropped 40 ft (12 m) onto a concrete pad to determine whether they could be initiated by impact. A total of six drop tests were conducted using either vertical, horizontal, or 45-degree orientations. Figure 12A shows the drop-test setup.

Drop tests 1 and 2 involved an 8-ft (2.4-m) long, 5-5/8-in (0.14-m) diameter canister. They were end-on drops with bottom impact (normal downhole direction), with RIP ignitors exposed, and with EBW initiators not installed. In each test the canister bounced twice on the concrete pad and fell across the pad edge, breaking near its

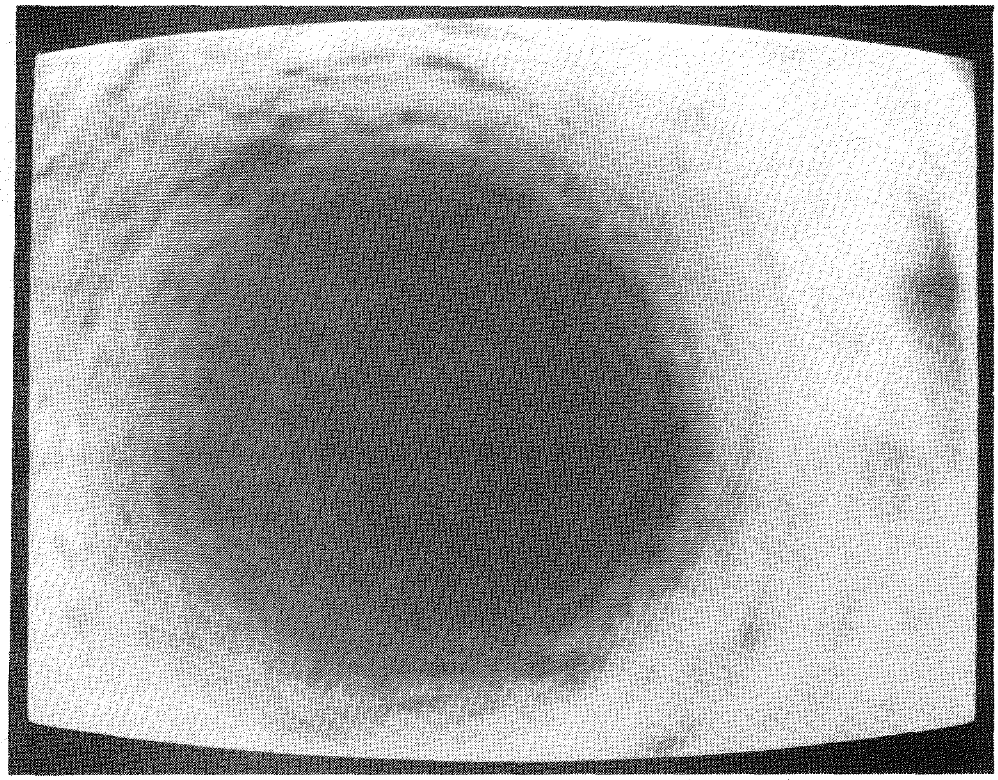

PRETEST WELLBORE

POSTTEST WELLBORE

Figure 11. Pictures from Downhole TV Camera

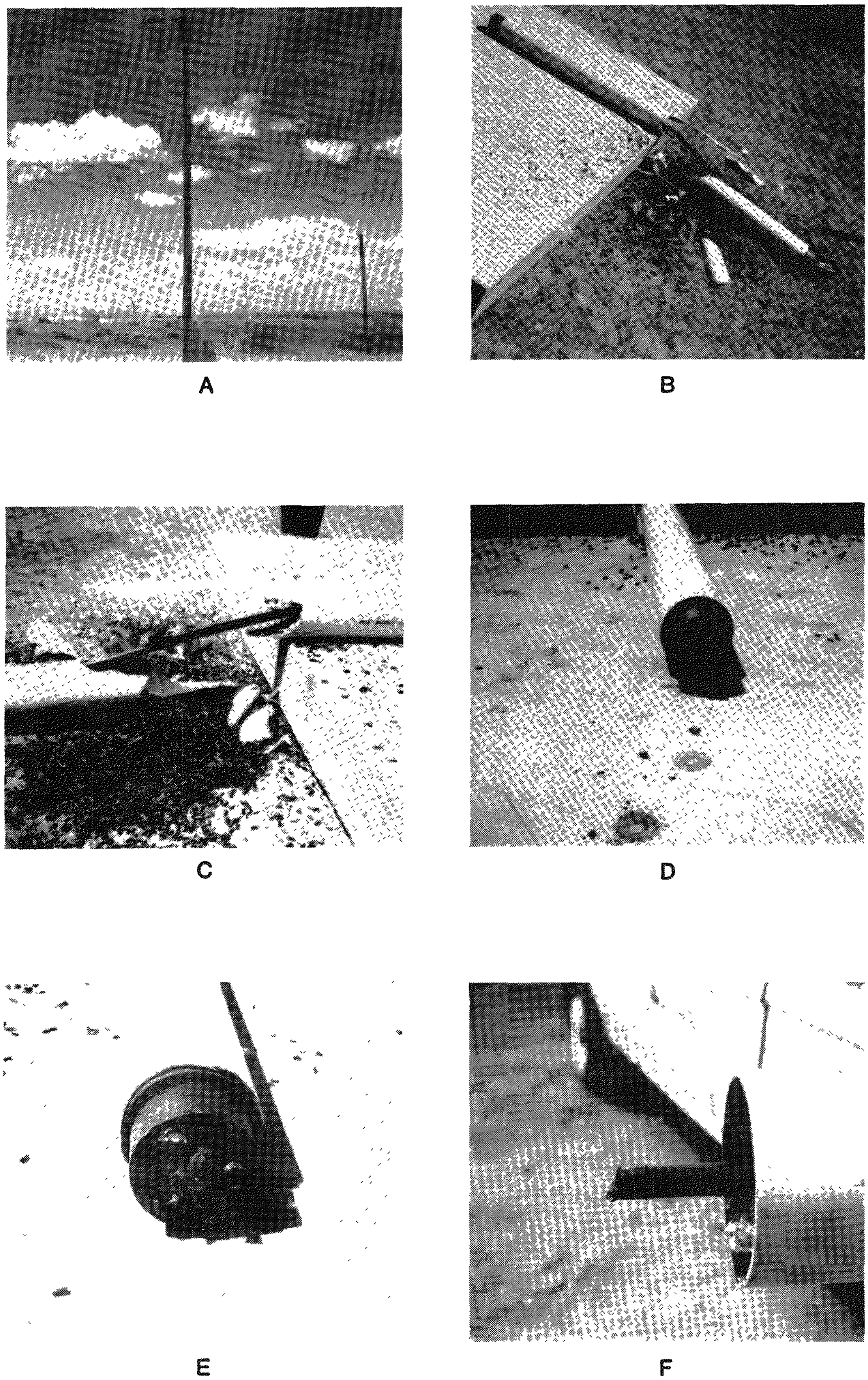

Figure 12. Photographs of Drop Tests 1 and 2

(A) Propellant canister suspended on lanyard 40 ft (12 m) above concrete pad prior to drop test.

(B) Broken propellant canister resulting from end bounce and fall across pad edge.

(C) Closeup of (B) showing scattered propellant and intact RIP ignitor.

(D) Double impact marks on pad from end of RIP ignitor housing.

(E) End view of propellant canister showing impacted end.

(F) Side view of exposed RIP ignitor after removal of PVC endcap; the PVC weld between endcap and tubing broke upon impact, making the endcap freely removable.

Figure 12

middle and spilling propellant onto the pad and surrounding ground. The bottom tubing-to-endcap PVC weld also broke, and propellant escaped from around the end of the RIP ignitor. No initiation occurred. The RIP ignitor remained intact. Figures 12B through 12F summarize the results from drop tests 1 and 2.

Drop test 3 used a 2-ft (0.61-m) long, 5-5/8-in (0.14-m) diameter canister dropped on its side. It shattered on impact, scattering propellant. The RIP ignitor remained intact, and no initiation occurred.

Drop test 4 was a repeat of 3. The canister again shattered. However, in this case the RIP ignitor also broke open, and $BKNO_3$ was scattered on the pad. The MDF center element was bent but intact. Again, no initiation occurred.

Drop test 5 used an 8-ft (2.4-m) long, 5-5/8-in (0.14-m) diameter canister that contained an EBW initiator installed at its top. Such a segment would be the topmost in a propellant-canister assembly. It was dropped end-on with the EBW initiator impacting on the concrete pad. The walls of the canister nearest the impacted end shattered, scattering propellant over the pad and surrounding ground. The RIP ignitor was twisted and broken in two, including the MDF. There was no initiation. The EBW initiator was successfully fired posttest. Figure 13 shows the results of drop test 5.

Drop test 6 used an 8-ft (2.4-m) long, 5-5/8-in (0.14-m) diameter canister, which was dropped with its axis at 45 degrees to vertical. It survived intact.

In summary, this series of tests demonstrated no evidence of an initiation hazard due to impact.

4.2.2.2 Burn Tests -- A series of three tests involving exposure of propellant canisters to JP-4 fuel fires was completed at Sandia's Lurance Canyon Burn Facility. The purpose of the tests was to observe and record the behavior of propellant-canister segments in a fully

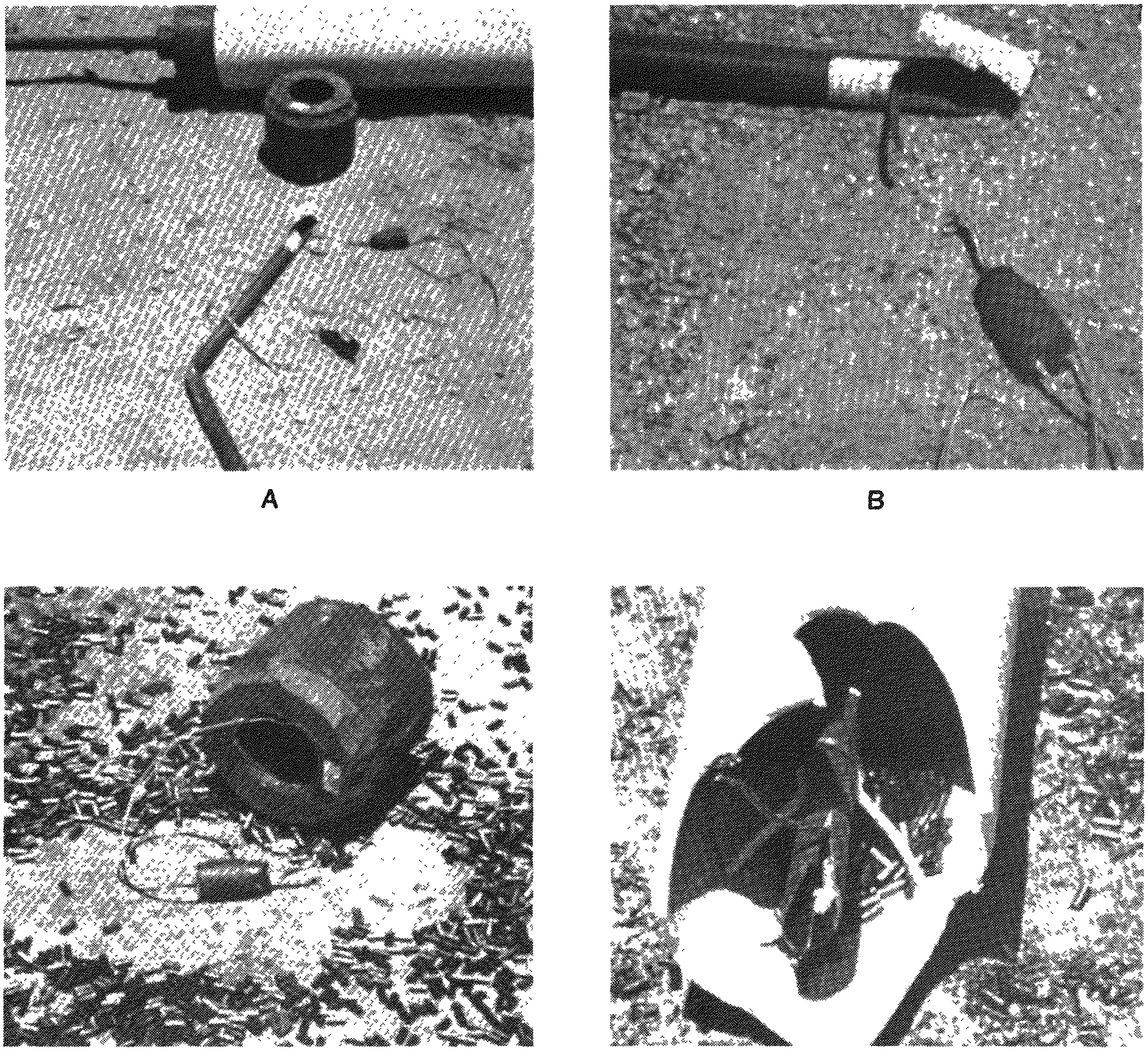

A B C D

(A) Overview of propellant-canister components, including unshattered top portion of propellant canister, EBW initiator, bottom PVC mating endcap, and broken lower half of RIP ignitor.

(B) Broken RIP ignitor with EBW initiator still attached, after removal from propellant canister.

(C) Close-up of EBW initiator, bottom PVC mating endcap, and scattered propellant.

(D) End view of severed propellant-canister section, showing broken RIP ignitor.

Figure 13. Photographs of Results of Drop Test 5

engulfing fire representative of an accidental fire situation. Figure 14 is photographs and Figure 15 is a schematic of the burn-test setup.

The test apparatus consisted of a fuel tub, a canister-support stand, and an air-curtain system. The fuel tub, 6 ft (1.8 m) in diameter and 2 ft (0.61 m) deep, was filled with water to a level 8 in (0.2 m) below its top lip. A layer of JP-4 fuel 1-1/2 in (0.038 m) deep was added, giving a total burn time of approximately 10 minutes. The canister-support stand consisted of two 2-in (0.051-m) OD, 1/2-in (0.013-m) wall, stainless steel pipes placed in parallel across the diameter of the tub, to hold the propellant-canister segment approximately 8 in (0.20 m) above the fuel surface. The air curtain was used to protect the fire from wind effects and was produced by blowing 14,000 ft^3/min (6.6 m^3/s) of air from an annular area around the lip of the fuel tub. The fire was ignited remotely via an electric match and black-powder charge.

Two 30-ft (9.1-m) stadia poles were placed on opposite sides of the tub, in line with the canister-support stand. These poles were marked at 2-ft (0.61-m) intervals for use in estimating flame height. Two television cameras, placed 90° apart, were used--one provided a full frontal view of the canisters and stadia poles, and the other provided an end view. Figure 16 shows the approximate location of the video cameras and the stadia poles relative to the test apparatus.

In each of three tests (Table 1) a propellant-canister segment was burned in a JP-4 fuel fire: the first test with RIP-ignitor ends shielded to ensure burnthrough on the side of the canister, the second test with EBW initiator installed, and the third test with RIP-ignitor ends exposed. Figure 17 presents photographs of the burn sequence taken from the video record of Test 1; the times recorded in the lower left of each frame are in minutes and seconds from initiation of the electric match. In all three tests, the canister was breached in roughly 2 minutes, with a resulting flash from the burning propellant lasting approximately 10 seconds. About 5 seconds after the end of the propellant burn, the RIP ignitor initiated.

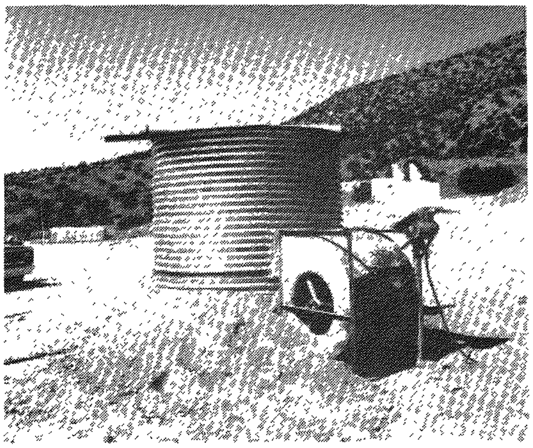

(A) Overview of test apparatus with propellant canister installed for test 1.

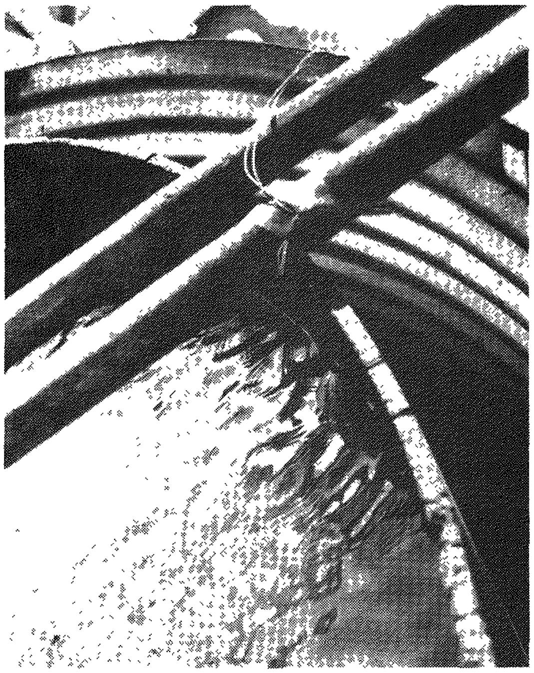

(B) Closeup of test apparatus showing the canister-support stand and the electric-match leads attached to black-powder charge (suspended just above JP-4 fuel surface).

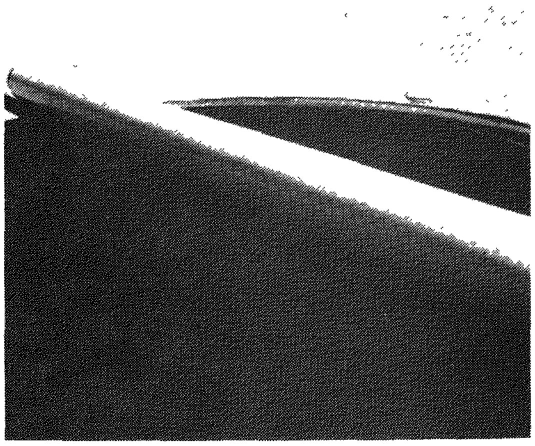

(C) Closeup of test apparatus with propellant canister installed for test 1.

Figure 14. Photographs of Burn-Test Setup

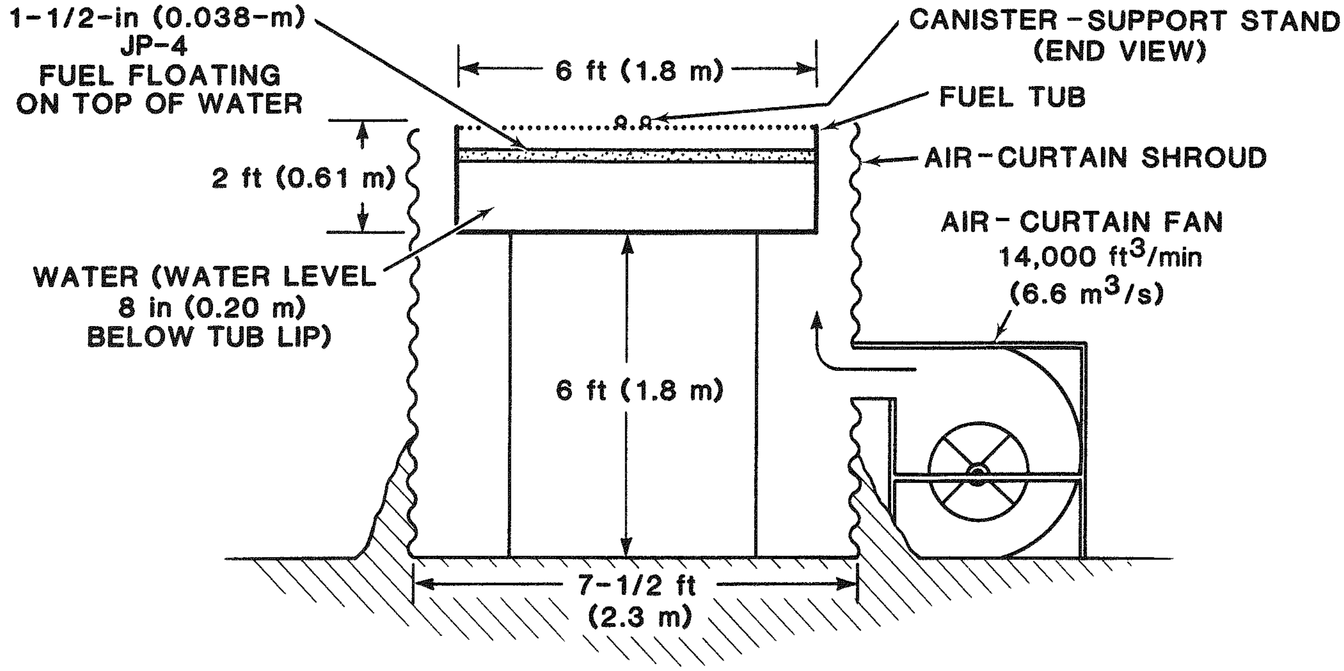

Figure 15. Schematic of Burn-Test Apparatus

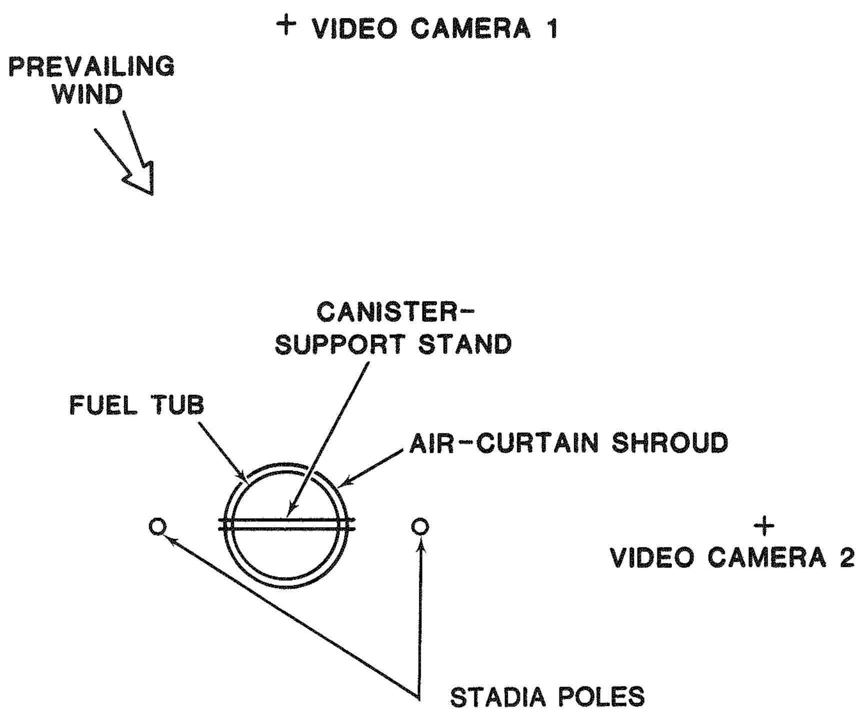

Figure 16. Plan-View Schematic of Burn-Test Area

Table 1

Summary of Burn Tests

Test No.	Diameter	Propellant Canister Length (in) (m)	End Configuration	Outer Canister Burnthrough (s)	Propellant Burnout (s)	Ignitor Burnthrough (s)	Note
1	5-5/8-in (0.14 m) OD PVC pipe	96 (2.4)	Unprotected but not in flames	118	129	135	RIP ignitor initiated
2	3-in (0.076 m) PVC pipe	24 (0.61)	EBW initator on one end, other end capped	87	110	111	RIP ignitor did not initiate
3	5-5/8-in (0.14 m) OD PVC pipe	24 (0.61)	Unprotected in flames	139	149	163	RIP ignitor initiated

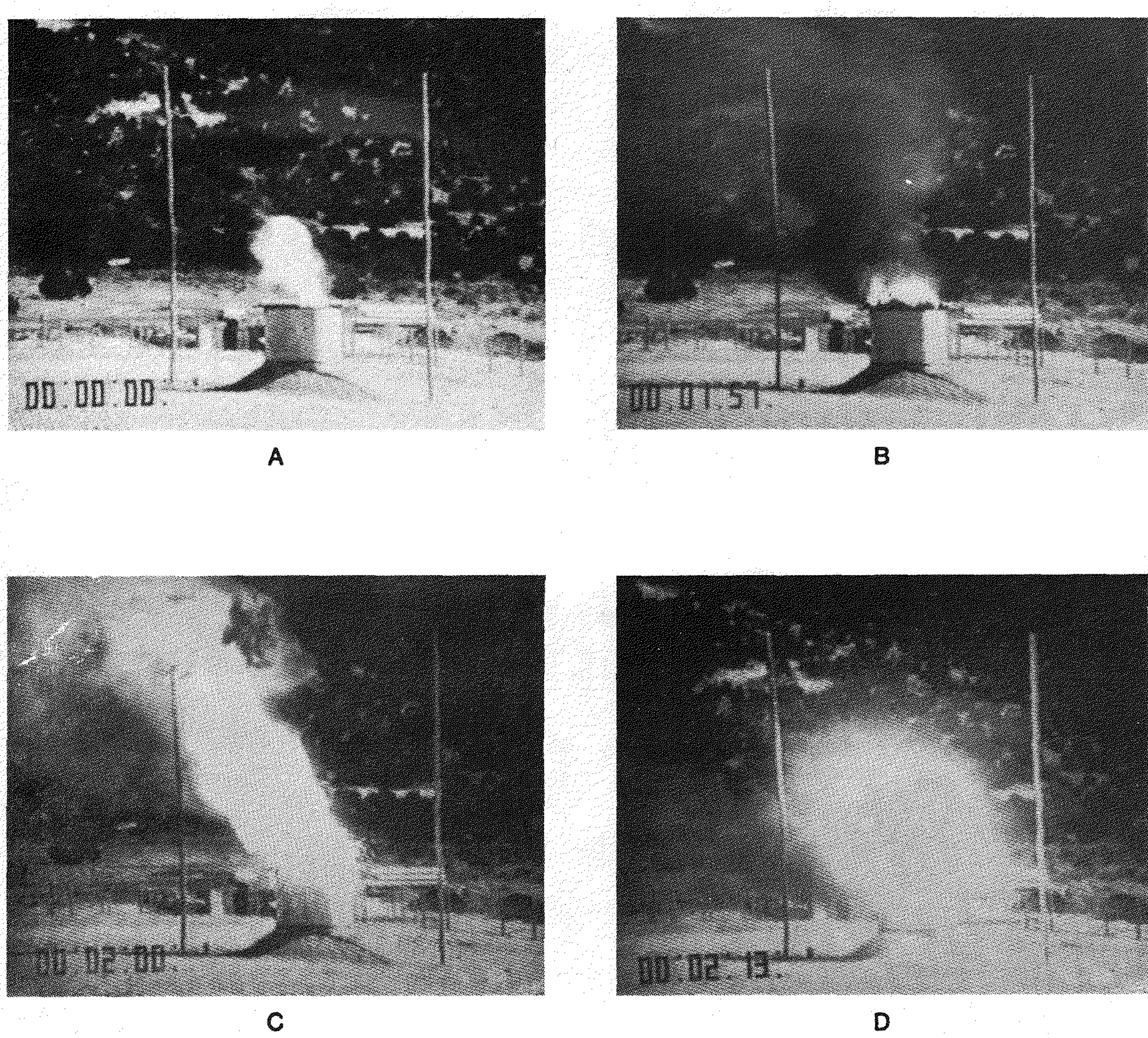

(A) Initiation of JP-4 fuel.

(B) Background level from burning JP-4 fuel.

(C) Flash from propellant burn when propellant canister was breached.

(D) Initiation of RIP ignitor (one to two second flash after which the fire returned to background level as seen in [B]).

Figure 17. Selected Frames from Video Record of Burn Sequence in Burn Test 1

Flames produced by the burning JP-4 fuel were about 4 ft (1.2 m) high. With burnthrough of the propellant-canister wall, the flames and burning propellant spewed up about 30 ft (9.1 m). Similar behavior occurred when the RIP ignitors initiated. An additional consequence of the RIP-ignitor initiation was that molten plastic spewed out over an approximately 20-ft (6.1-m) radius.

In summary, the danger resulting from a fire in which propellant-canister segments burn does not appear substantially greater than if an equal amount of unconfined propellant were burned. The only additional consequence appears to be dispersal of molten plastic over a limited area.

4.2.3 Refinements to the Semiempirical Model and Its Applications

During this quarter, modeling activities focused on developing a simple model to predict the effect on pressure risetime of increasing the annular volume surrounding a propellant canister. The resulting model was combined with semiempirical relationships developed previously[2-5] to specify a propellant mixture that leads to multiple fracturing. To describe the model and its application, the model is discussed within the context of the procedure used to determine the propellant mixture that will produce multiple fracturing in the proof test.

4.2.3.1 Scaling Risetime with Changes in Free Volume -- The proof test differed from previous experiments in that the annulus surrounding the propellant canister was enlarged to ensure that the package would not hang up on emplacement. This required a 6-3/4-in (0.17-m) diameter borehole. The only previous experiment in ash-fall tuff employing a 5-5/8-in (0.14-m) OD propellant canister was GF4 of the MultiFrac series, which was done in a 6-in (0.15-m) diameter borehole. In the proof test, the total free volume (propellant-canister void space plus the annular volume between borehole and propellant canister) per unit length was more than 2.5 times that in GF4. The effect of increasing free volume is to increase the pressure risetime for a given propellant mixture. It was thus necessary to specify a faster-burning propellant mixture than was used in GF4 (100% M5[B]) to obtain a comparable risetime in the proof test.

A scaling relationship was derived that quantified the effect on pressure risetime of increasing or decreasing the free volume. It was assumed that the burn-rate equation for M5 propellant holds during the risetime, t_m, to peak pressure, P_m, and that the volume remained constant during that period. This assumption is equivalent to saying that negligible fracture volume is produced during the risetime to peak pressure. The burn-rate equation is given as

$$R = aP^n \tag{1}$$

where

R = burn rate (m/s)
a = linear burn-rate coefficient
P = pressure (Pa)
n = pressure exponent (0.81 for M5 propellant).

It is noted that the propellant-gas-production rate, dm/dt (kg/s), is proportional to the rate at which the propellant burns. Thus,

$$\frac{dm}{dt} = bP^n \tag{2}$$

where b is the new proportionality constant.

Assuming ideal gas behavior, the relationship between pressure, volume, temperature, and amount of propellant gas produced in the wellbore during the test is given by

$$PV = m \frac{R}{M} T \tag{3}$$

where

P = gas pressure
V = free volume
m = mass of propellant gas in volume V
R = gas constant
T = burn temperature (assumed constant at 3000 K)
M = molecular weight of the gas.

Differentiating with respect to time, assuming constant free volume and burn temperature, yields

$$\frac{dP}{dt} V = \frac{dm}{dt} \frac{R}{M} T \tag{4}$$

Substituting bP^n for dm/dt (Equation 2) and rearranging results in

$$\frac{MV}{RT} \frac{dP}{dt} = bP^n \tag{5}$$

Rearranging and integrating gives

$$\frac{MV}{bRT} \int_0^{P_m} P^{-n} \, dP = \int_0^{t_m} dt \tag{6}$$

where P_m is peak pressure and t_m is pressure risetime. Then

$$\frac{MV}{bRT} \frac{P_m^{1-n}}{1-n} = t_m \tag{7}$$

Setting n = 0.81 (Equation 1) results in

$$P_m^{0.19} V = (\text{Constant}) \, t_m \tag{8}$$

which makes it possible to calculate the pressure risetime, t_{m_2}, in a borehole of known free volume, V_2, given the risetime, t_{m_1}, in a different borehole of known free volume, V_1 (for the same propellant mixture and the same size propellant canister). More specifically,

$$\frac{P_{m_1}^{0.19} V_1}{P_{m_2}^{0.19} V_2} = \frac{t_{m_1}}{t_{m_2}} \tag{9}$$

Because of the weak pressure dependence ($P_m^{0.19}$), one can scale simply from the relationship

$$\frac{t_{m_1}}{t_{m_2}} \approx \frac{V_1}{V_2} \tag{10}$$

4.2.3.2 Risetimes for Multiple Fracturing -- Before specifying a propellant mixture for the proof test, it was necessary to determine the pressure risetime that could be expected to produce multiple fracturing in the 6-3/4-in (0.17-m) diameter borehole. As has been previously established,[2-5] a suitable pressure risetime must fall within the interval,

$$\pi D/2C_R < t_m < 8\pi D/C_R \qquad (11)$$

where t_m = pressure risetime, D = borehole diameter, and C_R = surface-wave velocity. The curves that have been shown to bound the multiple-fracturing regime are plotted in Figure 18. This figure shows that for a 6-3/4-in (0.17-m) diameter borehole, pressure risetimes between 0.26 ms and 4.2 ms can be expected to produce multiple fracturing. For the proof test, a pressure risetime of 0.5 ms was selected.

4.2.3.3 Specification of Propellant Mixture for the Proof Test Experiment -- Figure 19 shows the experimentally determined variation of pressure risetime with borehole diameter, for propellants M5(A) and M5(B). For a given borehole diameter, any pressure risetime between that for pure M5(A) propellant and that for pure M5(B) propellant can be obtained by a proper mixture of the two. A formula for calculating the mixture of the two propellants that obtains a desired pressure risetime, t_m, was presented in a previous report.[5] A more rigorous formulation is presented here. Although both formulations give the same fraction of M5(A) for t_m greater than about 0.3 ms, the previous derivation underestimates the fraction of M5(A) required for risetimes faster than 0.3 ms.

Results from several mixed-propellant experiments indicate that for a constant borehole diameter, the risetime varies logarithmically from one pure propellant to the other. Moreover, the interval from M5(A) to M5(B) is the same at any borehole diameter, hence the parallel lines in Figure 19. As a result, for a given borehole diameter, the logarithm of the risetime t_m for a mixture of the two propellants can be expressed as a single linear relationship between the logarithms of the risetimes t_A and t_B for the pure propellants M5(A) and M5(B). This relationship can be expressed in normalized form by

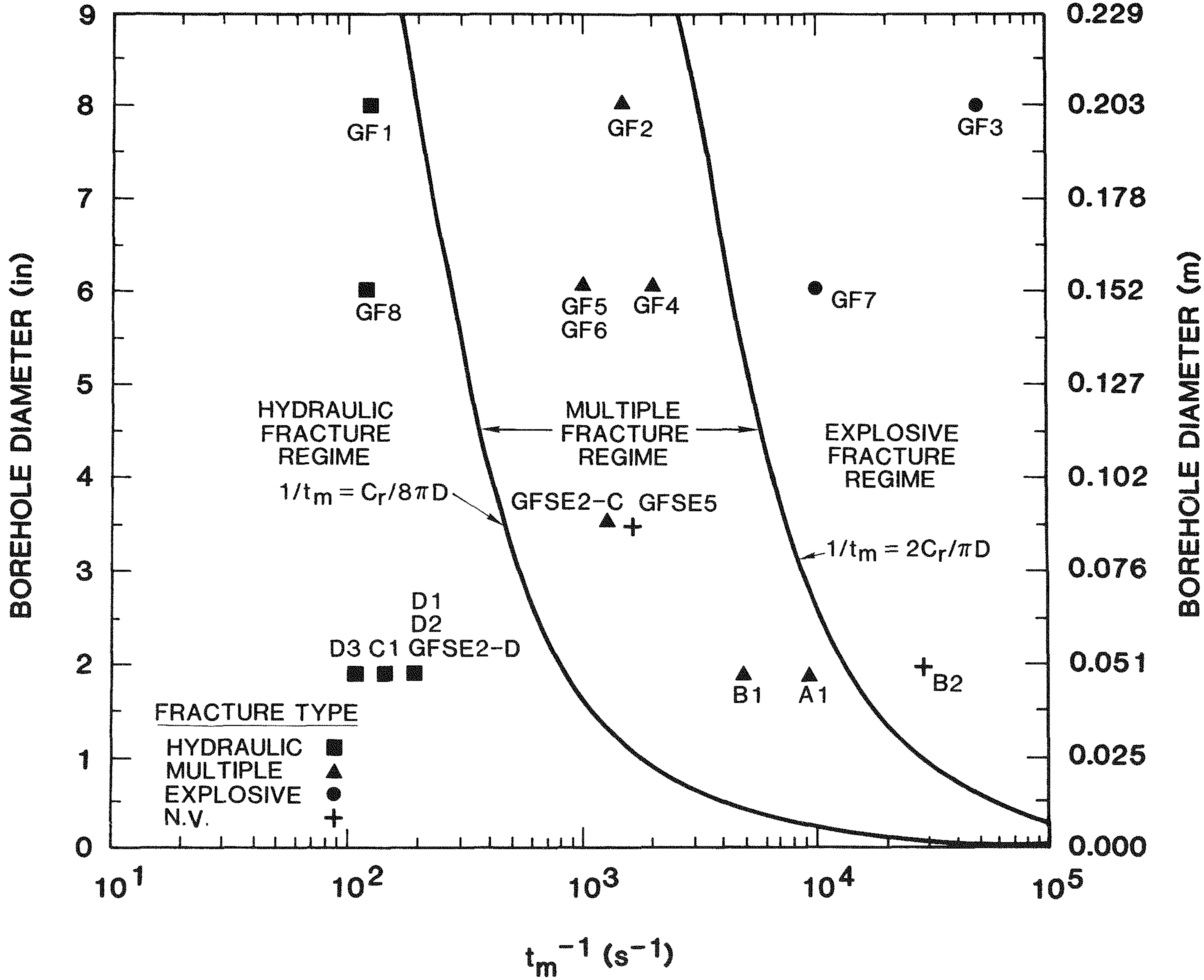

Figure 18. Fracture Regimes as Predicted by Semiempirical Modeling

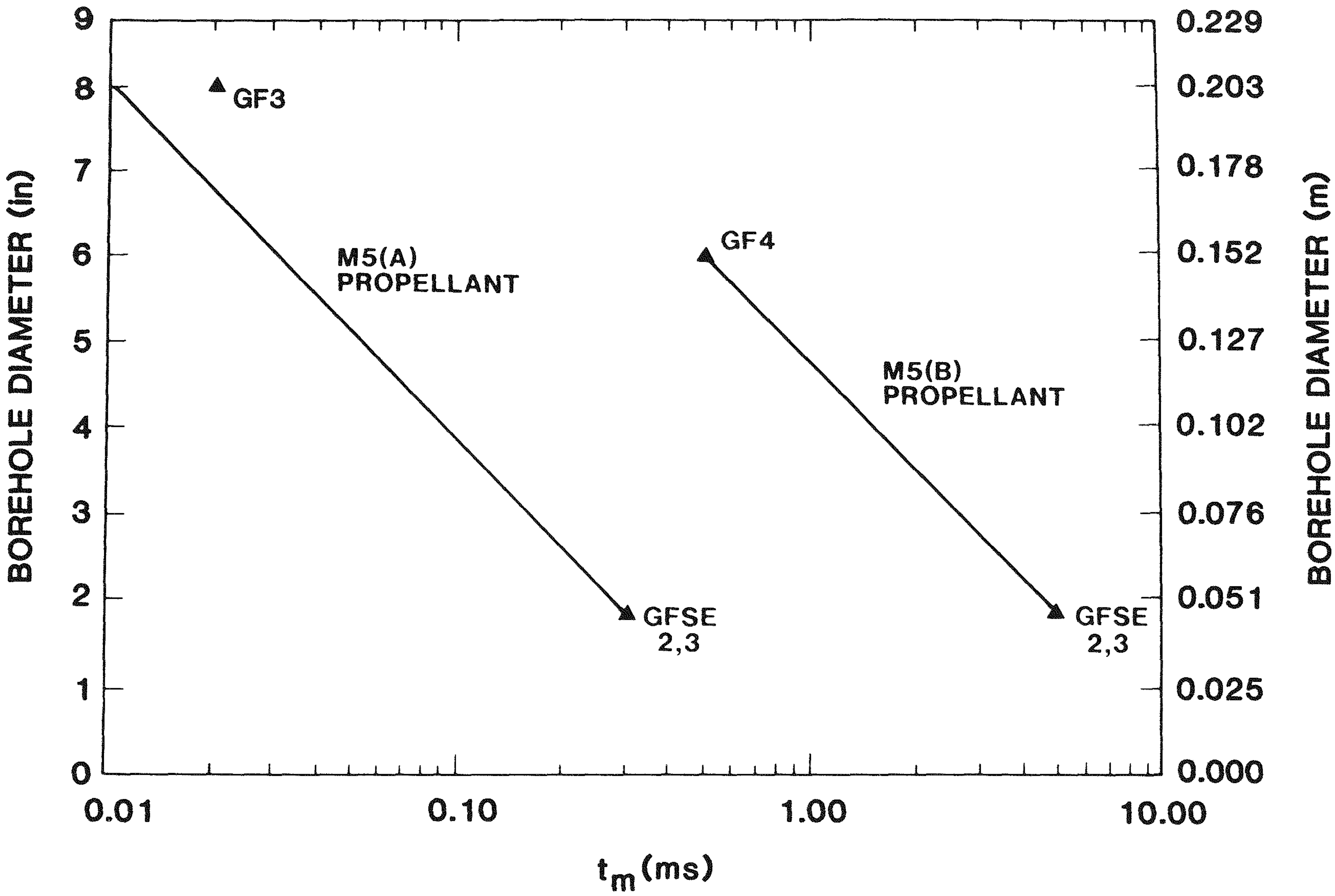

Figure 19. Pressure Risetime as a Function of Propellant and Borehole Diameter

$$\log t_m = \frac{A \log t_A + B \log t_B}{A + B} \qquad (12)$$

where the constants A and B are proportional to the weight fractions f_A and f_B of pure propellants M5(A) and M5(B) in the mixture (i.e., A = af_A and B = bf_B, with a and b being constants).

Equation 12 may be rewritten to give

$$\log t_m = \frac{af_A \log t_A + bf_B \log t_B}{af_A + bf_B} \qquad (13)$$

and rearranged, using $f_A + f_B = 1$ and $a/b = k$, to give

$$f_A = \frac{\log \frac{t_B}{t_m}}{\log \frac{t_B}{t_m} + k \log \frac{t_m}{t_A}} \qquad (14)$$

The constant, k, was determined empirically from several experiments that used mixed propellants. It was found to be approximately 2. Thus, the mixing formula becomes

$$f_A = \frac{\log \frac{t_B}{t_m}}{\log \frac{t_B}{t_m} + 2 \log \frac{t_m}{t_A}} \qquad (15)$$

Before calculating f_A for the proof test, it was necessary to determine t_B and t_A for the larger free volume in the proof-test borehole. From Figure 19, one obtains for a 6-in (0.15-m) diameter borehole (that of GF4) t_B = 0.5 ms and t_A = 0.03 ms. In the proof test, the free volume was approximately 15.4 in^3/in (9.94×10^{-3} m^3/m) while that of GF4 was about 5.9 in^3/in (3.8×10^{-3} m^3/m). Using Equation 10, the values of t_B and t_A can be corrected for the increase in free volume as follows:

$$t_B = (0.5 \text{ ms}) \frac{15.4}{5.9} = 1.3 \text{ ms}$$

and

$$t_A = (0.03 \text{ ms}) \frac{15.4}{5.9} = 0.08 \text{ ms}$$

Substituting these values, and $t_m = 0.5$ ms (the desired risetime in the proof test), into Equation 15 yields $f_A = 0.2$. Thus, a propellant containing 20 percent M5(A) and 80 percent M5(B) by weight was used in the proof test.

5. NEXT QUARTER (JANUARY - MARCH 1983)

5.1 Work Planned for Next Quarter

5.1.1 Selection of Sites for Devonian Shale Experiments

Negotiate to obtain one or more acceptable sites for full-scale experiments in Devonian shale. The two leading candidates are sites in Rowan County, Kentucky, and Miegs County, Ohio.

5.1.2 Improvement in the Design of the Firing Module

Relocate the firing module from the top of the pressure-transducer canister to a position above the tamp-emplacement canister. This places the firing module above the sand tamp and reduces costs by simplifying recovery and making reuse of the firing module possible.

5.1.3 Design of a Downhole Tool for Postshot Hardware Recovery

Design a washover tool to latch onto the top of the cable tube to retrieve it and the pressure transducer, thus reducing well clean-up costs. This requires redesign of the top of the cable-tube assembly.

5.1.4 Fabrication of a Well-Testing Appartus

Fabricate a well-test apparatus that will allow measurements of natural-gas flow rates and pressure buildup within a particular interval of a wellbore.

5.1.5 Completion of Gap Tests

Test approximately 30 different gaps between propellant-canister pairs to statistically determine maximum acceptable gaps.

5.1.6 Finite-Element Model Refinements

Incorporate treatment of gas dynamics and rock response to propellant burn into the finite-element model.

5.1.7 Image Transformation of Television Log

Sandia's 54° wide-angle borehole TV camera confirmed multiple fracturing in the proof test. Image processing is being examined as a possible tool for additional characterization of fracture widths and spacing.

5.2 Next Quarter's Work Relative to Overall Work Plan

Table 2 summarizes the current schedule for the program, which must be regarded as tentative, pending approval for well-site access. Because sites for the full-scale experiments in Devonian shale are not yet designated, they are identified generically as the "shallow" site and the "deep" site.

Table 2

Current Schedule

	Task	Dates
1)	Modify hardware a) Move firing module above tamp-emplacement canister b) Integrate squib firing module with relocated firing module c) Design washover tool/cable tube interface	January 1-March 30
2)	Test above unit at NTS	April 1-April 30
3)	Design, fabricate, and test well-testing apparatus	January 1-March 30
4)	Install stressmeters and accelerometers at the "shallow" site	February 15-April 1
5)	Drill test well at the "shallow" site	April 1-May 1
6)	Conduct full-scale experiments at the "shallow" site	May 1-July 1
7)	Conduct full-scale experiments at the "deep" site	July 1-July 31
8)	Continue advanced modeling	January 1-October 1
9)	Enhance images from borehole TV camera	January 1-October 1
10)	Analyze system performance	January 1-October 1

ACKNOWLEDGEMENTS

Useful discussions with D. A. Northrop and N. R. Warpinski are gratefully acknowledged. A large number of individuals in Sandia National Laboratories' field-engineering, test, and support organizations, and NTS support organizations contributed to the reported results. These include J. T. McIlmoyle, field-experiment project leader; P. W. Cooper, explosive consultation; A. C. Arthur, D. Fogel, and S. P. Breeze, mechanical design and installation; J. P. Johnson, R. L. Peabody, W. C. Wilson, and F. Shoemaker, explosives arming and firing; J. J. Laukota, L. A. Kracko, R. V. Peet, G. S. Worthen, and C. D. Lucas, data acquisition; C. W. Cook and E. A. Ames, instrumentation; R. J. Dye, NTS project coordinator; L. R. Carrillo, J. Hallock, and J. S. Talbutt, NTS field and tunnel support; D. W. Shadel, D. Denning, and J. Neel, NTS borehole-TV logging; L. Arnold, NTS still photography; J. P. Weber, R. E. Bohannon, D. A. Luna, and W. R. Geck, canister drop tests; and W. Gill, W. R. Drake, W. W. Gravning, R. F. Gardner, and R. C. Ezell, canister burn tests.

REFERENCES

1. Swenson, D. V., Taylor, L. M., "Analysis of Gas Fracture Experiments Including Dynamic Crack Formation," SAND82-0633, Sandia National Laboratories, to be issued.

2. Cuderman, J. F., "Design and Modeling of Small Scale Multiple Fracturing Experiments," SAND81-1398, Sandia National Laboratories, December 1981.

3. Cuderman, J. F., Cooper, P. W., Northrop, D. A., in Proc. 1981 International Gas Research Conf., September 28 - October 1, 1981, Los Angeles, CA.

4. Cuderman, J. F. "Multiple Fracturing Experiments--Propellant and Borehole Considerations," Proceedings 1981 SPE/DOE Symposium on Unconventional Gas Recovery, May 16-18 1982, Pittsburgh, PA.

5. Cuderman, J. F., High Energy Gas Fracturing Development, Annual Report, April 1981 - March 1982, GRI 80/0144; SAND82-0866, April 1982.

DISTRIBUTION:

John C. Sharer
Director
Natural Gas Supply Research
Gas Research Institute
8600 W. Bryn Mawr Avenue
Chicago, IL 60631

Timothy D. Kurtz (30 copies)
Manager
Devonian Shale Research
Gas Research Institute
8600 W. Bryn Mawr Avenue
Chicago, IL 60631

Javaid Alam
Science Applications, Inc.
Suite 8
Chestnut Ridge Prof. Bldg.
Chestnut Ridge Road
Morgantown, WV 26505

Natural Gas Pipeline Company
of America (2)
122 So. Michigan Avenue
Chicago, IL 60603
Attn: Michael J. Birch
Stanley D. Whatford

Porter J. Brown
Chief Geological Services
Columbia Gas Transmission Corp.
P.O. Box 1273
Charleston, WV 25325

Joseph E. Campbell
Director
Oil & Special Projects
Columbia Gas Transmission Corp.
1700 MacCorkle Avenue, S.E.
Charleston, WV 25314

Public Service Electric
& Gas Co. (2)
80 Park Place
Newark, NJ 07101
Attn: Paul D. Chase - Rm T16A
Carol A. Stephens -
LaBrie - Rm 12330

Robert W. Christopher
Director of Research and
Development
United Gas Pipe Line Co.
P.O. Box 1478
Houston, TX 77001

Robert M. Forrest
Manager, Supply Research
Columbia Gas System Service Corp.
1600 Dublin Road
P.O. Box 2318
Columbus, OH 43216-2318

Ernest C. Geer
Chief Engineer--Process Design
Transco Energy Co.
P.O. Box 1396
Houston, TX 77001

Lone Star Gas Co. (2)
301 South Harwood Street
Dallas, TX 75201
Attn: Billy D. Brown
David P. Giebelhaus

Robert D. Habbit
El Paso Natural Gas Company
P.O. Box 1492
El Paso, TX 79978

Vello A. Kuuskraa
Executive Vice President
Lewin and Associates, Inc.
1090 Vermont Ave. N.W.
Suite 700
Washington, DC 20005

TXG Resources, Inc. (2)
P.O. Box 1160
Owensboro, KY 42301
Attn: Forrest W. Lewis, VP
R. Mark Berry, Geologist

John L. Moore
System Chief Production Engineer
Consolidated Natural Gas Service
Company
Four Gateway Center
Pittsburgh, PA 15222

DISTRIBUTION (Continued):

Lawrence Pakenas
Project Associate
New York State Energy Research
and Development Authority
Agency Building 2
Empire State Plaza
Two Rockefeller Plaza
Albany, NY 12223

Stephen E. Foh
Manager, Gas Storage Research
Institute of Gas Technology
3424 South State Street
Chicago, IL 60616

Alfred E. Schlemmer
Research Advisor
Texas Eastern Gas Pipeline Corp.
P.O. Box 2521
Houston, TX 77001

Nicholas J. Skorski
Area Geologist
American Natural Resources Co.
717 17th Street, Suite 2500
Denver, CO 80202

Harry L. Steadman
Senior Vice President
National Fuel Gas Supply Corp.
10 Lafayette Square
Buffalo, NY 14203

Harry Stout
Senior Vice President
Marketing & Gas Supply
Florida Gas Transmission Company
P.O. Box 44
Winter Park, FL 32790

Brooklyn Union Gas Company (2)
195 Montague Street
Brooklyn, NY 11201
Attn: Joseph A. Vaszily - Rm 1308
Anthony J. Giuliani

Ronald E. Zielinski
Energy Systems Technology Manager
Monsanto Research Corporation
Mound Facility
Miamisburg, OH 45342

U.S. Department of Energy (2)
Office of Oil, Gas & Shale Technology
Mail Stop D-107
Washington, DC 20545
Attn: E. J. Lievens, Jr.
P. R. Wieber

U.S. Department of Energy (3)
Morgantown Energy Technology Center
P.O. Box 880
Morgantown, WV 26505
Attn: A. A. Pitrolo
A. E. Hunt
C. A. Komar

U.S. Department of Energy (4)
Bartlesville Energy Technology Center
Bartlesville, OK 74003
Attn: H. C. Johnson
D. C. Ward
A. B. Crawley
H. B. Carroll

U.S. Department of Energy
Nevada Operations Office
P.O. Box 14100
Las Vegas, NV 89114
Attn: C. H. Atkinson

U.S. Department of Energy
Special Programs Division
Albuquerque Operations Office
Albuquerque, NM 87185
Attn: D. L. Krenz, Director

Earth Sciences Division, L200 (2)
Lawrence Livermore National Laboratory
University of California
P.O. Box 808
Livermore, CA 94550
Attn: Robert P. Swift
Merle Hanson

Los Alamos National Laboratory
MS 740
Los Alamos, NM 87545
Attn: Nick Vanderborgh

DISTRIBUTION (Continued):

CER Corporation
P.O. Box 15090
Las Vegas, NV 89114
Attn: R. L. Mann

Amoco Production Co.
P.O. Box 591
Tulsa, OK 74102
Attn: R. W. Veatch

John A. Bartol, Director
Systems Studies
Applied Engineering Resources, Inc.
114 East de la Guerra Street
Santa Barbara, CA 93101

F. Glenn Martin
Atlantic Richfield Company
P.O. Box 2819
Dallas, TX 75221

George Stoiber
Bounty Oil & Gas Inc.
2 E. Second Street
Jamestown, NY 14701

Charles Callery
Callery Exploration Company
2422 Bank of the Southwest Bldg.
Houston, TX 77002

Jeff Gentry
Constitution Petroleum Co. Inc.
Suite 1020 Newhouse Bldg.
10 Exchange Place
Salt Lake City, UT 84111

Continental Oil Company (2)
Production Research Division
Ponca City, OK 74601
Attn: H. C. Walther
H. Wahl

R. Steanson
Dowel
P.O. Box 21
Tulsa, OK 74102

Linn Coursen
Petrolchemical Department
Potomac River Laboratory
E. I. DuPont Inc.
Martinsberg, WV 25401

John Gidley
Exxon Company USA
P.O. Box 2180
Houston, TX 77001

T. W. Muecke
Exxon Production Research Co.
P.O. Box 2189
Houston, TX 77001

A. R. Sinclair, President
Fracturing Technology, Inc.
10301 N. W. Freeway
Suite 202
Houston, TX 77092

R. P. Trump
Gulf Research & Development Co.
P.O. Drawer 2038
Pittsburgh, PA 15230

Halliburton Services (2)
Research Center
Duncan, OK 73533
Attn: A. A. Daneshy
A. B. Waters

Spencer C. Watson
Manager of Planning and Analysis
Room 1161C
Hercules Inc.
910 Market Street
Wilmington, DE 19899

Kim Lilly
Lilly Oil Company
P.O. Box 1885
Paso Robles, CA 93446

Doy Jones
President
Texas Exploration Drilling Co.
P.O. Box 1310
Claremore, OK 74017

H. G. Kozik
Mitchell Energy Corp.
2001 Timberlock Place
The Woodlands, TX 77380

DISTRIBUTION (Continued):

J. L. Fitch
Mobil Research & Development Corp.
Field Research Laboratory
P.O. Box 900
Dallas, TX 75211

Ralph L. Coates
Director of Research
Mountain Fuel Supply, Inc.
P.O. Box 11368
Salt Lake City, UT 84139

S. H. Advani, Chairman
Dept. of Engineering Mechanics
Ohio State University
Boyd Laboratory
155 West Woodruff Avenue
Columbus, OH 43210

Arthur Spencer
Petroleum Technology Corporation
P.O. Box 537
Redmond, WA 98052

E. T. Moore, Jr.
Physics International
2700 Merced St.
San Leandro, CA 94577

Chapman Young
Science Applications, Inc.
P.O. Box 88010
Steamboat Springs, CO 80488

R. Saucier
Shell Development Company
1 Shell Square
701 Poydras Street
New Orleans, LA 70139

David L. Holcomb
Director of Technology
Smith Energy Services
Timberline Building
Junction Hwys 58 & 93
Golden, CO 80401

L. F. Elkins
SOHIO Petroleum Co.
50 Tennessee Place
Suite 1100
Oklahoma City, OK 73118

Douglas D. Keough
Stanford Research Institute
333 Ravenswood Avenue
Menlo Park, CA 94025

Thomas A. Edgell, President
Super Frac Inc.
P.O. Box 8244
Tyler, TX 75711

TerraTek (2)
University Research Park
420 Wakara Way
Salt Lake City, UT 84108
Attn: R. A. Schmidt
A. S. Abou-Sayed

H. M. Stoller (2)
TPL Inc.
3409 Bryn Mawr NE
Albuquerque, NM 87107

Edgar A. Rassinier
Director Resource Planning
Trunkline Gas Company
P.O. Box 1642
Houston, TX 77001

C. W. Spencer
U.S. Geological Survey
Box 25046
MS 951
Denver Federal Center
Denver, CO 80225

Fred W. Schwerer, P.E.
United States Steel Corporation
Research Laboratory
125 Jamison Lane
Monroeville, PA 15146

J. Reed Holland
School of Mines and Energy Development
University of Alabama
P.O. Box 6282
Tuscaloosa, AL 35486

W. L. Fourney
Department of Mechanical Engineering
University of Maryland
College Park, MD 20742

DISTRIBUTION (Continued):

Arthur M. Van Tyne
P.O. Box 326
Wellsville, NY 14895

K. J. Touryan
Mount Morieh Trust
6200 Plateau Dr.
Englewood, CO 80111

1 G. C. Dacey
1520 T. B. Lane
1524 W. H. Sullivan
1524 D. V. Swenson
1524 L. M. Taylor
1540 W. C. Luth
Attn: B. M. Butcher, 1542
3153 R. C. Colgan
Attn: R. F. Gardner, 3153
W. W. Gravning, 3153
7000 O. E. Jones
Attn: C. D. Broyles, 7100
7110 J. D. Plimpton
Attn: C. R. Mehl, 7112
7112 C. W. Smith
7116 S. R. Dolce
Attn: C. W. Cook, 7116
7120 T. L. Pace
7123 B. C. Benjamin
7123 R. V. Peet
7123 D. Fogel
7123 G. S. Worthen
7125 G. L. Ogle
7125 J. T. McIlmoyle
7125 A. C. Arthur
7130 J. D. Kennedy
7131 B. G. Edwards
7131 R. J. Dye
7131 L. R. Carrillo
7131 V. E. Kerr
7131 D. W. Shadel
7131 J. S. Talbutt
7132 A. Church
7132 P. W. Cooper
7133 R. D. Statler
7133 W. C. Wilson
7533 F. H. Mathews
Attn: W. Gill, 7533
J. P. Weber, 7533
9530 R. W. Lynch
Attn: L. D. Tyler, 9537
9000 G. A. Fowler
9700 E. H. Beckner
9740 R. K. Traeger
Attn: J. R. Kelsey, 9741
P. J. Hommert, 9747
J. T. Schamaun, 9747
9750 V. L. Dugan
Attn: H. M. Dodd, 9752
B. W. Marshall, 9755
D. Engi, 9756
9753 D. A. Northrop
9753 J. F. Cuderman (25)
9753 J. C. Lorenz
9753 A. R. Sattler
9753 N. R. Warpinski
8214 M. A. Pound
3141 L. J. Erickson (5)
3151 W. L. Garner (3)

For DOE/TIC (Unlimited Release)
DOE/TIC (25)
(3154-4 C. H. Dalin)